

RNA helicase DDX6 and scaffold protein GW182 in P-bodies promote biogenesis of stress granules

Vladimir Majerciak^{1,*}, Tongqing Zhou², Michael J. Kruhlak³ and Zhi-Ming Zheng^{1,*}

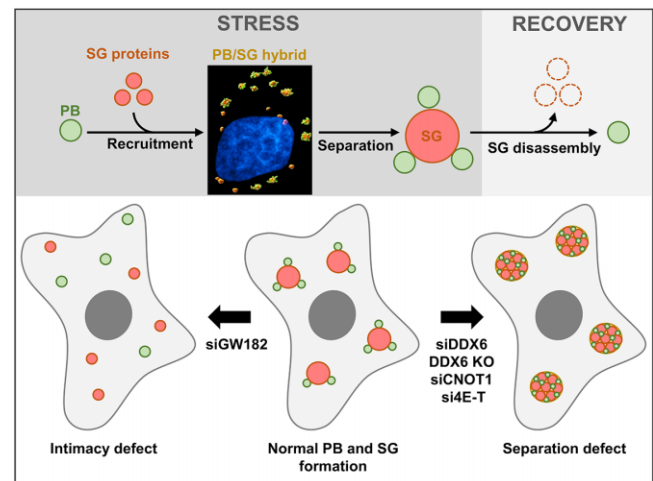
¹Tumor Virus RNA Biology Section, HIV Dynamics and Replication Program, National Cancer Institute, National Institutes of Health, Frederick, MD 21702, USA, ²Structural Biology Section, Vaccine Research Center, National Institute of Allergy and Infectious Diseases, National Institutes of Health, Bethesda, MD 20892, USA and ³CCR Confocal Microscopy Core Facility, Laboratory of Cancer Biology and Genetics, National Cancer Institute, National Institutes of Health, Bethesda, MD 20892, USA

Received October 20, 2021; Revised June 05, 2023; Editorial Decision June 15, 2023; Accepted July 07, 2023

ABSTRACT

Two prominent cytoplasmic RNA granules, ubiquitous RNA-processing bodies (PB) and inducible stress granules (SG), regulate mRNA translation and are intimately related. In this study, we found that arsenite (ARS)-induced SG formed in a stepwise process is topologically and mechanically linked to PB. Two essential PB components, GW182 and DDX6, are repurposed under stress to play direct but distinguishable roles in SG biogenesis. By providing scaffolding activities, GW182 promotes the aggregation of SG components to form SG bodies. DEAD-box helicase DDX6 is also essential for the proper assembly and separation of PB from SG. DDX6 deficiency results in the formation of irregularly shaped ‘hybrid’ PB/SG granules with accumulated components of both PB and SG. Wild-type DDX6, but not its helicase mutant E247A, can rescue the separation of PB from SG in DDX6KO cells, indicating a requirement of DDX6 helicase activity for this process. DDX6 activity in biogenesis of both PB and SG in the cells under stress is further modulated by its interaction with two protein partners, CNOT1 and 4E-T, of which knockdown affects the formation of both PB and also SG. Together, these data highlight a new functional paradigm between PB and SG biogenesis during the stress.

GRAPHICAL ABSTRACT



INTRODUCTION

Cytoplasmic membrane-less RNA-processing bodies (PB) and stress granules (SG) are two of the best-studied, common RNA granules. Both consist of translationally arrested mRNAs in complex with numerous RNA-binding proteins (RBP) and, therefore, are associated with translational control in eukaryotic cells (1). Despite their functional overlaps, PB and SG have been thought in profound differences of their composition, assembly, and dynamics.

The smaller PB occur in every cell under physiological conditions and are ubiquitous from yeast to humans (2). PB, free from 40S ribosomal subunits, are derived from the condensation of various ribonucleoprotein (RNP) complexes, including ~125 RBP (3). Two-thirds of PB-associated RBP are functionally linked to mRNA repression, RNA decay, miRNA-mediated silencing, RNA decapping, and non-sense mediated RNA decay (NMD) (3–6). However, it becomes increasingly clear that PB are not the

*To whom correspondence should be addressed. Tel: +1 301 846 6170; Email: majerciv@mail.nih.gov
Correspondence may also be addressed to Zhi-Ming Zheng. Tel: +1 301 846 7634; Email: zhengt@exchange.nih.gov

sites of mRNA degradation (7–12) and mainly function as the sites of translational repression of AU-rich, nonoptimal codon-enriched mRNAs encoding proteins with regulatory functions (13,14). The mRNA translational repression in PB is independent of miRNA-mediated silencing (9,12). In fact, mRNAs in the PB are actually protected from decay and become translatable after release from PB (3,15–17). Interestingly, the mRNAs encoding housekeeping proteins and long non-coding RNAs (lncRNAs) are generally excluded from PB (3). PB-specific protein markers including GW182, DDX6, 4E-T, DCPIA, DCP2 and EDC3 are commonly used by different groups to visualize PB in cells (8,12,18,19).

The larger SG contain 40S ribosomal subunits and appear in the cells only under stress conditions (20). Cells under both biological (hypoxia, nutrients deprivation, or viral infection) and environmental (changes in temperature or osmotic pressure) stress or exposure to certain chemicals (sodium arsenite or ARS, chemotherapy compounds, etc.) can be induced to form SG due to the rapid increase of translationally arrested mRNAs released from polysomes (21–24). Different types of stress which activate four different eIF2 α kinases (GCN2, PKR, PERK and HRI) (25–29) have a common influence by inducing the phosphorylation of an essential translation initiation factor eIF2 α at Ser51 position (22,30). Heterotrimeric eIF2, which is composed of eIF2 α , eIF2 β and eIF2 γ , binds GTP and the initiator methionine-tRNA (tRNA^{iMet}) as an eIF2-GTP-tRNA^{iMet} complex and loads the tRNA^{iMet} onto the small 40S ribosomal subunit by hydrolysis of eIF2-GTP to eIF2-GDP. Phosphorylation of eIF2 α leads eIF2 to stably bind eIF2B, a guanine exchange factor and sequester of eIF2B activity, thus inhibiting the recycling of eIF2-GDP to eIF2-GTP by eIF2B and blocking the formation of preinitiation complexes and protein translation (31–33). Consequently, translationally stalled mRNAs with bound small ribosomal subunits are then recognized by G3BPs and TIA1 nucleators for SG assembly (22,34–37). A chemical inhibitor antagonizing the effects of phospho-eIF2 on eIF2B restores translation and causes SG disassembly (38). However, in some cases, a type II SG can be formed independently of eIF2 α phosphorylation (39,40). Conceivably, most SG protein components are involved in translation initiation and regulation and thus mechanistically, SG formation is driven by a high concentration of stalled preinitiation complexes recognized by SG nucleating RBP, such as G3BP1, TIA1 and others, which bind both RNA and small ribosomal subunits and thus mediate multivalent interactions to facilitate SG condensation and recruitment of additional factors (34,35,37). These multivalent nucleation interactions cause liquid-liquid phase separation (LLPS) to form SG and can be regulated by a G3BP-binding CAPRIN1 to promote, or another G3BP-binding USP10 to prevent, SG formation (36). To date, thousands of different mRNA species with relatively long coding and UTR regions and ~411 RBP have been identified in purified SG from the cells under stress (14,41). However, it appears that the mRNAs within the SG are not degraded and become translatable after recovery from stress (17). An ATR4 reporter RNA was found to be translatable even within the SG itself (42). RNA-binding proteins TIA1, G3BP1, and PABPC1 are SG-specific mark-

ers and useful for visualizing SG in cells under various stress conditions.

Even through PB and SG are distinct, they are dynamically linked sites of RNP remodeling and share some of their components (14,43). How PB in cells under physiological conditions and SG in the cells under stress are formed are only partially understood (44). It is known that PB commonly increase in number and size in the stressed cells and often appear in close physical proximity with SG; however, their intimate relationship is not fully understood and the role of PB in SG formation is highly debated and somewhat confusing. Some propose that translationally arrested RNPs are first targeted to SG, where they are remodeled, stripped of translational components, and transferred to PB for storage and degradation (4,45–47). Some suggest that two RNA granules are independent, because the inhibition of SG formation did not prevent PB formation (46). Others argue that PB and SG are only temporarily intimately related when PB are ‘docked’ to SG, allowing content exchange (43). Several proteins were identified to promote PB docking on SG, such as TTP and CPEB1 (43,48). A recent finding of single mRNAs interacting with both SG and PB and moving bi-directionally between SG and PB further supports the intimate relation of PB with SG (49). PB were also found to promote SG formation in yeast (50). Recent observation of overlapping proteomes between PB and SG and complex interactions between multiple PB and SG components (4,43,51,52) further support this notion. Both PB and SG are enriched in RBP containing, intrinsically disordered regions (IRD) or prion-like domains (PrD) (53–55). These RBP at high local concentration mediate multivalent protein-RNA, protein-protein, and RNA-RNA interactions that lead to LLPS (56). Microscopic studies showed that both granules represent highly dynamic structures, rapidly exchanging their components with the surrounding environment (43,45) and involving ATP-dependent rearrangement of RNP (53,57). Several ATP-dependent RNA helicases are enriched in both PB and SG (3,4,57,58). Their ability to modulate the RNP composition was proposed to contribute to PB and SG dynamic nature (57,59). However, the direct role of PB in SG biogenesis has not been adequately addressed.

DEAD-box helicase 6 (DDX6/p54/Rck and its orthologues Dhh1 in *S. cerevisiae*, Me31B in *D. melanogaster*, CGH-1 in *C. elegans* and Xp54 in *X. laevis*) is one of the ATP-dependent, cellular RNA helicases containing a conserved Asp-Glu-Ala-Asp motif (DEAD-box) and other high levels of sequence and structure conservations (50,60–63). DDX6 consists of an N-terminal and a C-terminal RecA-like domain for interactions with various factors for specific functions and ATP-binding/ATPase and RNA-binding/helicase activities (64). DDX6, abundantly expressed in cells, is highly interactive with RNAs and almost half of all PB proteins (3,8,65). Thus, DDX6 is essential for PB formation (12) and retaining PB identity during stress (66). Interestingly, while ATPase activity is essential for PB assembly, this activity of DDX6 appears not affecting the existing PB (19). The top interactors of DDX6 include members of mRNA decay and translational repression complexes (8). The C-terminal RecA-like domain of DDX6 mediates most of DDX6 protein-protein interac-

tions, such as interactions with PATL1, CNOT1, and 4E-T in regulating PB formation (8,67,68). Although DDX6 is a cofactor of XRN1 5'–3' exonuclease and its interaction with PATL1 affects RNA 3' to 5' degradation, recent reports indicate no RNA decay or degradation within the PB (3,15–17) and CNOT1-mediated physiological mRNA degradation occurs predominantly outside of PB (69,70). While these protein-protein and protein-RNA interactions seem sufficient for DDX6 to act as a central node, it becomes increasingly clear that DDX6 RNA-helicase activity appears essential for *de novo* PB formation (19,71).

Although the exact intimate nature between PB and SG is yet to be understood, both contain translationally repressed RBP and shared exchangeable components (43). In this study, we investigated the contribution of PB to SG formation in cells in response to arsenite (ARS) treatment. We found that SG are formed in a stepwise process from smaller SG cores into larger granules as stress progresses. SG aggregation is topologically linked to PB and requires PB-associated scaffold protein GW182. DDX6, a PB-associated DEAD-box RNA-helicase, also participates in the formation of SG and is required for separating PB from SG. Loss of DDX6 or its helicase activity is detrimental for both PB and SG biogenesis, leading to the formation of irregular shape of 'hybrid' PB/SG granules during cellular stress. DDX6 activity is further regulated by its interacting partners, CNOT1 and 4E-T. Thus, a direct role of several PB components was identified in SG biogenesis in this report.

MATERIALS AND METHODS

Cells

HeLa cells (CCL-2, ATCC, Manassas, VA) were maintained in Dulbecco's modified Eagle's medium (DMEM, cat. # 12430054, Thermo Fisher Scientific, Waltham, MA). HAP1 wild type (WT) and DDX6 knockout (KO) cells (HZGHC000116c001, Horizon Discovery, Cambridge, UK), which were originally derived from human chronic myelogenous leukemia (CML) cell line KBM-7, were maintained in Iscove's modified Dulbecco's medium (IMDM, Thermo Fisher Scientific). All media were supplemented with 10% fetal bovine serum (FBS, cat. # SH30070.03, Hyclone, Cytiva, Marlborough, MA) and 1× Penicillin–Streptomycin–Glutamine (PSG, cat. # 10378016, Thermo Fisher Scientific). The cells were kept at 37°C in a humidified atmosphere containing 5% CO₂.

Stress induction

To induce stress granule formation, cells were incubated in the complete culture medium (DMEM or IMDM with 10% FBS and 1× PSG) supplemented with 0.5 mM sodium arsenite (ARS, cat. # 1062771003, Sigma Aldrich, St. Louis, MO) for 0–30 min. Cells without ARS treatment were used as a negative control.

siRNA knockdown

HeLa cells at 0.25×10^6 were plated into 6-well plates 24 h before the first siRNA transfection with 40 nM of the

ON-TARGETplus human siRNA SMARTpool (Horizon Discovery) using LipoJet (cat. # SL100468, SigmaGen Laboratories, Frederick, MD) as recommended by the manufacturer. Twenty-four hours after the siRNA transfection, the cells were split into two wells with glass coverslips. Four hours later, the cells were transfected again with the same siRNA at 40 nM, followed by an additional 24 h incubation before the stress induction. HAP1 cells at 0.15×10^6 were plated directly on the cover glass and transfected once with 40 nM of siRNA for 24 h. ON-TARGETplus human siRNA SMARTpools (Horizon Discovery) targeting DDX6 (L-006371-00-0005), GW182 (TNRC6A, L-014107-00-0005), PATL1 (L-015591-01-0005), CNOT1 (L-015369-01-0005), 4E-T (EIF4ENIF1, L-013237-01-0005), EDC3 (L-017136-02-0005), TIA1 (L-013042-02-0005), and LSM14A (L-013920-02-0005) were used in this study. An ON-TARGET plus non-targeting siRNA #1 (siNT, D-001810-01-05, Horizon Discovery) was used as a negative control.

Complementation assay

The vector expressing myc-DDK-tagged-human WT DDX6 was purchased from OriGene (cat. # RC209431, Rockville, MD). The helicase-deficient DDX6 E247A mutant (MT) was constructed by overlapping PCR using primers oVM506 5'-ACTTATCTGCCGCATCCAATACTATCATCTGGACATGAT-3' and oVM507 5'-TTGGATGCGGCAGATAAGTTGCTGTACAGGATTTTGTG-3'. HAP1 DDX6KO cells grown on cover glass in 6-well plates were directly transfected with FLAG-tagged DDX6 WT or MT vectors. HeLa cells were first treated with non-targeting (siNT) or DDX6-targeting (siDDX6) siRNA twice at a 24 h interval. Two hours after the second siRNA transfection, the cells were transfected with the vector expressing either a WT or E247A mutant DDX6. The cells were then subjected to 0.5 mM ARS treatment for 30 min 24 h after vector transfection, followed by immunofluorescent staining.

Immunofluorescent (IF) staining

Cells grown on cover glass (–/+ ARS) were fixed with 4% paraformaldehyde (cat. #15710, Electron Microscopy Sciences, Hatfield, PA) in 1× PBS (phosphate buffered saline, pH 7.4, cat. # 10010023, Thermo Fisher Scientific) for 20 min at RT, followed by 5 min quenching with 100 mM glycine and permeabilization with 0.5% Triton X-100 (cat. # H5141, Promega, Madison, WI) in 1× PBS for 15 min. The cells were then washed three times with 1× PBS and blocked with 3% Blot-Qualified bovine serum albumin (BSA, cat. # W3841, Promega) in 1× PBS containing 0.05% Tween-20 (TPBS, cat. # AFF-J20605-AP, Thermo Fisher Scientific) in a humidified chamber for 1 h at 37°C. The primary (1:100) and AlexaFluor-labeled secondary antibodies (1:500, Thermo Fisher Scientific) were diluted in blocking solution and incubated with the slides in a humidified chamber at 37°C for 1–2 h. After each incubation, the slides were washed three times with TPBS. Hoechst 33342 (cat. # H3570, Thermo Fisher Scientific) was added to the last wash (1 µg/ml) to stain cell nuclei for 5 min. The fully

stained slides were mounted using ProLong Gold Antifade Mountant (cat. # P36934, Thermo Fisher Scientific) and let to cure overnight at room temperature.

Antibodies

The following primary antibodies were used in the study: human autoimmune serum containing anti-GW182 antibody were obtained as a gift from Dr. Marvin Fritzier University of Calgary; others were anti-DCP1A (cat. # ab183709, Abcam, Cambridge, MA), anti-TIA1 (clone OT1D7, cat. # MA5-26474, Thermo Fisher Scientific), anti-G3BP1 (cat. # 611126, BD Biosciences, Franklin Lakes, NJ), anti-DDX6 (cat. # NB200-191, Novus Biologicals, Centennial, CO), anti-CNOT1 (cat. # 14276-1-AP, Proteintech, Rosemont, IL), anti-PATL1 (cat. # A303-482A, Bethyl Laboratories, Montgomery, TX), anti-4E-T/eIF4E-T (cat. # A300-706A, Bethyl Laboratories), anti-LSM14A (cat. # 18336-1-AP, Proteintech), anti-EDC3 (cat. # 16486-1-AP, Proteintech), anti- β -tubulin (cat. # T5201, Millipore Sigma), rabbit anti-FLAG (cat. # F7425, Millipore Sigma).

Western blot

The cells transfected twice with non-targeting (siNT) or gene-specific siRNAs at a 24 h interval were harvested by direct lysis in 2 \times SDS protein samples buffer containing 5% (vol/vol) 2-mercaptoethanol. The obtained protein samples were separated on a 4–12% Bis-TRIS NuPAGE gel in 1 \times MES buffer (cat. # NP0002, Thermo Fisher Scientific) and transferred to a nitrocellulose membrane before blocking with 5% non-fat milk dissolved in 1 \times TRIS-buffered saline (TBS) containing 0.05% Tween-20 (TTBS). The membranes were stained with primary antibodies diluted 1:1000 in TTBS, followed by incubation with peroxidase-labeled secondary antibody (Millipore Sigma) diluted 1:10 000 in 2% non-fat milk in TTBS. The signal was developed by ProSignal Pico ECL Reagent (cat. # 20-300B, GeneSee Scientific, San Diego, CA) and processed by ChemiDoc Touch molecular imager (BioRad, Hercules, CA).

Image collection and processing

Images were acquired using a Nikon SoRa spinning disk microscope equipped with a 60 \times oil immersion objective lens (NA 1.49) and Photometrics BSI sCMOS camera. Super-resolution z-stacks were collected with 0.15 μm step-size and 0.027 μm x - y pixel size. The resultant images were deconvolved using a modified Richardson-Lucy iterative deconvolution algorithm in the Nikon Elements software (version 5.3), and then imported into Imaris image analysis software (version 9.9.0) where the different sub-cellular granules were segmented using automatic background subtraction setting to measure the number, size, and inter-granule distances. Alternatively, the subtraction was based on the different levels of the absolute signal intensity. GW182 staining objects with maximum intensity exceeding 1200 were counted as PB. Only the objects detected

by Imaris based on G3BP1 staining with a minimal volume of 0.2 μm^3 were considered as SG for statistical analysis. For those 'hybrid PB/SG clusters out of Imaris analytic resolution, manual counts were made for individual PB in each PB cluster and averaged from at least ten clusters (Supplementary Table S1). Otherwise, the confocal images were collected using the Zeiss LSM 880 confocal laser scanning microscope (Zeiss) with 63 \times oil immersion objective lens and processed by Zen image processing software (Zeiss). The 3D images were generated from respective z-stack images using the maximum intensity function. The ImageJ (<https://imagej.nih.gov>) was used to measure the signal intensity for individual channels at the cross-sections.

Statistical analysis

To test the statistical differences between two groups we used the two-tailed Student's t -test. For the comparison of three or more groups, we used a one-way ANOVA test with the Bonferroni correction. The linear regression analysis was used to calculate the association between two variables.

Structural modeling

The crystal structure of DDX6 (PDB ID: 5ANR) (67) was used to analyze the structural basis of E247A mutation. Briefly, the domain 1 (DEAD domain) of DDX6 was superposed with the corresponding domain of RNA helicase DDX3X at pre-unwound state (PDB ID: 6O5F) (72) to show the relative locations of the DEAD domain and helicase domain with RNA bound. Since the DEAD sequence is a Walker B motif that has been shown to be critical in the binding and hydrolysis of ATP, a non-hydrolysable ATP analog, ATP- γ -S, and an Mg^{2+} critical for ATP hydrolysis were modeled into the DDX6 ATP-binding site based on alignment with the crystal structure of Ski2 RNA-helicase Brr2 (PDB ID: 6QV4) (73). Structural alignment, modeling and graphical rendering were carried out with PyMol Molecular Graphics System, version 2.4.1 (www.pymol.org).

RESULTS

Kinetics of SG biogenesis during ARS-induced stress

Previous observations suggested a close topological, biochemical, and functional connection between PB and SG (1,4,43). However, the mechanistic role PB play in SG formation remains elusive. To determine whether any PB components contribute to SG formation, we performed a time-course study of SG biogenesis in HeLa cells after exposure to ARS (0.5 mM), a well-studied chemical SG inducer, for 0, 5, 10, 15, 20 and 30 min, followed by staining for the markers of PB (GW182) and SG (TIA1). As shown in Supplementary Figure S1, HeLa cells at both time 0 and 5 min of ARS induction exhibited \sim 4–5 large and \sim 10–15 smaller rounded GW182-positive PB as previously reported (12) but no detectable SG. At this stage, TIA1 was stained as a diffused cytoplasmic protein with some nuclear appearance. By 10 min, but more profoundly, by 15 min, we observed the initial appearance of granular TIA1 staining in the cytoplasm of ARS-treated cells, accompanied by an increased

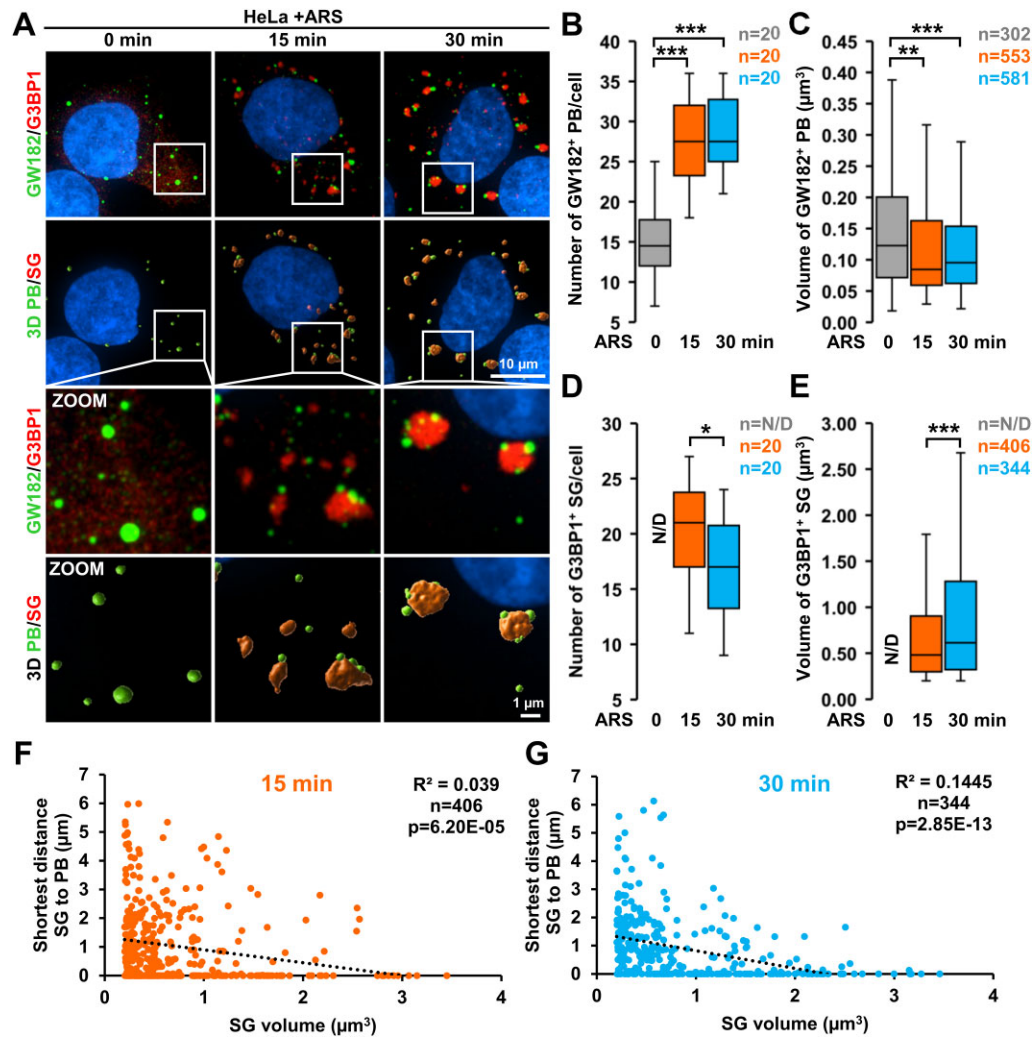


Figure 1. PB promotes the stepwise biogenesis of SG during ARS-induced stress. (A) HeLa cells were treated with 0.5 mM arsenite (+ARS) for 0, 15 and 30 min, followed by staining with anti-GW182 and anti-G3BP1 antibodies. Super-resolution z-stack images were used to generate a 3D model of PB (GW182 staining) and SG (G3BP1 staining) using Imaris image analysis software. (B–E) Number per cell (B, D) and volume (C, E) of PB (B, C) and SG (D, E) detected in 20 randomly selected HeLa cells at time 0, 15 and 30 min after arsenite (+ARS) treatment. The box plots in B–E show the median (–), minimum and maximum (whiskers), *** $P < 0.001$, ** $P < 0.01$, * $P < 0.05$ by Student *t*-test. (F, G) Correlation between SG volume and shortest distance to the closest PB detected in 20 HeLa cells at 15 and 30 min after the arsenite treatment. The circles represent individual data point and dotted lines the calculated trendline. Linear regression was used to calculate R^2 and P -value.

number of small PB. Interestingly, most newly formed SG appeared within close physical proximity to PB, with mature SG often surrounded by multiple PB (see zoom in 30 min time point). However, most but not all PB were associated with SG. To perform a quantitative analysis of this process, we developed an image-based 3D modeling on PB and SG. Fixed cells were stained for GW182 and G3BP1 to mark PB and SG, respectively. Super-resolution z-stacks were acquired and the volume rendering and segmentation of both PB and SG could be obtained by Imaris image analysis software using an automatic background threshold setting. The numbers of PB and SG per cell, PB and SG volumes, mutual distances, and signal intensities of individual markers were obtained for each cell and used for further statistical analysis. We then used this method to confirm the link between PB and SG biogenesis observed in our initial time-course study by quantification of PB and SG in HeLa cells treated

with ARS for 0, 15, and 30 min. As shown in Figure 1A, at 0 min, most cells contained ~15 PB/cell, as previously reported (12) (Supplementary Table S2) and as expected, no SG, with G3BP1 exhibiting diffused cytoplasmic staining. At 15 min after ARS treatment, the number of PB almost doubled to ~28 PB/cell (Figure 1B), but ARS-induced PB were overall in smaller size (Figure 1C), even though several large PB were also observed. The newly formed SG were clearly detectable with ~21 SG/cell at 15 min (Figure 1A and D, Supplementary Table S2). At 30 min, the number and volume of PB remained similar to that observed at 15 min (Figure 1B and C). However, the number of SG significantly decreased to ~17 SG/cell on average at 30 min (Figure 1D). Inversely, average SG size significantly increased between 15 min and 30 min of ARS treatment (Figure 1E, Supplementary Table S2). As observed in our initial time-course study (Supplementary Figure S1), almost all large

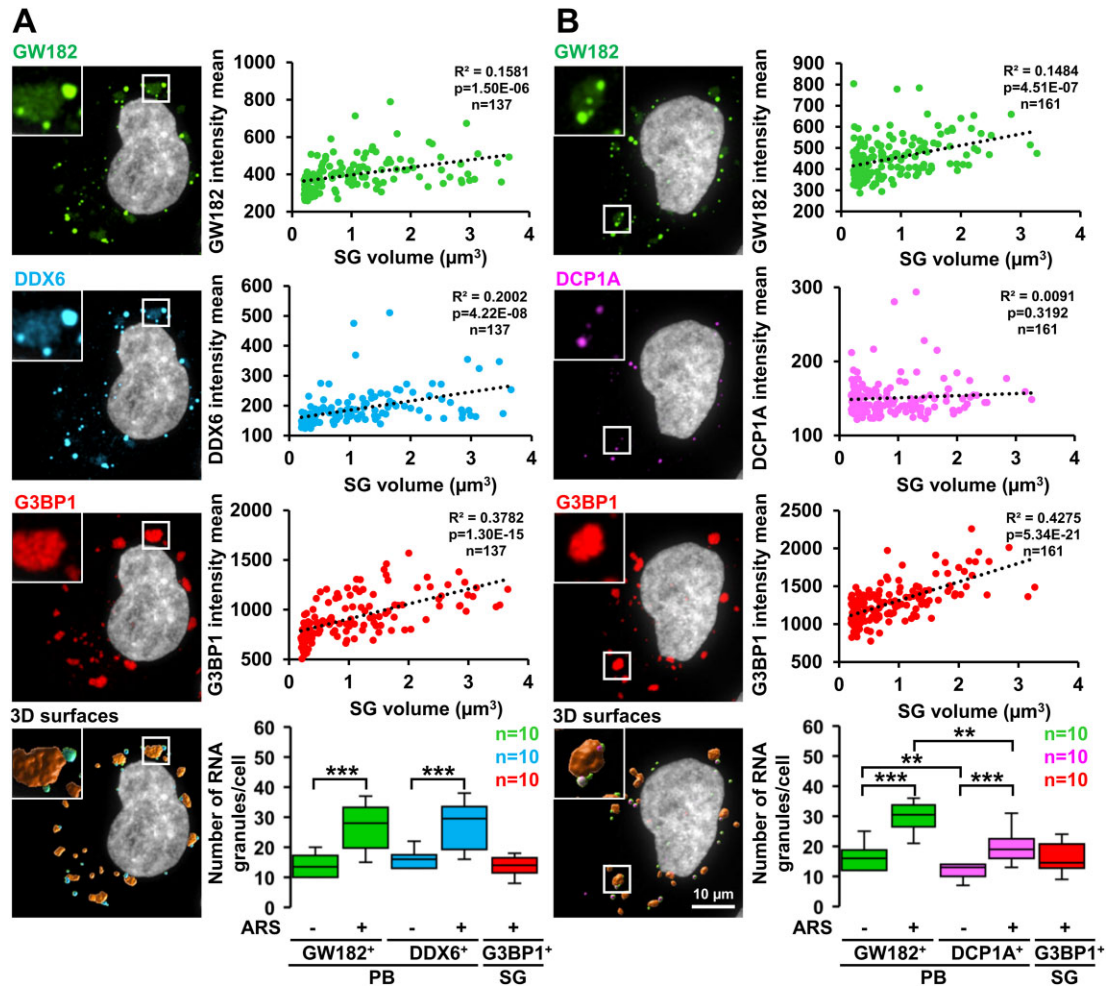


Figure 2. PB components are selectively recruited to SG. (A, B) HeLa cells without or with 30 min treatment with 0.5 mM arsenite (+ARS) were stained with an anti-G3BP1 for SG and anti-GW182 along with anti-DDX6 (A) or anti-DCP1A (B) antibody for PB. The SG 3D model based on G3BP1 staining was generated by Imaris software based on the z-stack images of 10 randomly selected cells in each group. The mean signal intensity means for each marker in detected SG was plotted alongside the volume of individual SG (top panels). The dotted lines represent the calculated trendline. The linear regression was used to calculate R^2 and P -value. The GW182, DDX6 or DCP1A signal was used to generate the 3D model of PB in the same cells to determine the number of PB per cell (lower panels, *** $P < 0.001$, ** $P < 0.01$ by Student t -test).

SG were associated with PB although not every PB was linked to SG (Figure 1A). By counting the number of associated PB per SG, we found an increase from ~ 1 PB/SG at 15 min to ~ 2 –3 PB/SG at 30 min (Supplementary Table S1). The measured distance between SG and PB confirmed a negative correlation between SG volume and distance to the closest PB at both 15- and 30-min time points, thus supporting our observation (Figure 1F and G). Together, these data suggest that SG are formed by a stepwise process likely starting from small ‘core’ SG aggregating/growing into fewer larger granules in the vicinity of PB, indicating a possible role of PB components in this process.

Selective accumulation of PB components in the newly formed SG

A close examination of GW182 staining in ARS-treated cells showed that SG growing into a larger size is not only topologically linked to PB but also associated with GW182 accumulation in SG (Supplementary Figure S1).

This was confirmed by the observation of GW182 in overlapping with G3BP1-positive SG in HeLa cells under ARS stress (Supplementary Figure S2) and the measurement of GW182 signal intensity in the G3BP1-positive SG in 10 randomly selected ARS-treated HeLa cells (Figure 2A and B). Interestingly, we observed a significant positive correlation between GW182 signal intensity and SG size (Figure 2A and B). We next asked if other PB components also accumulate in SG similarly to GW182. We chose two additional, commonly used PB-specific markers, DDX6, an RNA-helicase, and DCP1A, an mRNA-decapping enzyme 1A (8). We found that DDX6 also accumulates significantly in the SG, and like GW182, its signal intensity was overlapped with G3BP1 and positively correlated significantly with SG size (Figure 2A, Supplementary Table S3). Both DDX6 and GW182 were highly overlapped in PB and thus gave an almost identical number of detected PB both in the absence or presence of stress (Figure 2A, lower bar graph panel, Supplementary Table S3). In contrast, DCP1A was excluded from SG and DCP1A signal intensity showed no

correlation with SG size (Figure 2B). Even though the number of DCP1A-positive PB also increased slightly during the stress, their number was significantly lower than that of GW182-positive PB and appeared independently of stress condition, indicating that not every RNA in the PB has a cap for DCP1A binding and, unlike DDX6, DCP1A is present only in a fraction of PB (Figure 2B, Supplementary Table S3) as reported (69,74). The lack of functionality associated with PB (9) and its localization inconsistent with the localization of other PB components strongly argue against the reliable use of DCP1A as a PB marker. Together, these data suggest that multiple PB components selectively accumulate in newly formed SG under stress condition, which is consistent with the previously reported partial overlap in PB and SG proteomes (4).

Direct roles of GW182, DDX6 and other PB components in SG formation

Given the close topological correlation between PB and SG (Figure 1) and selective accumulation of PB components GW182 and DDX6 in SG (Figure 2, Supplementary Figure S2), we performed siRNA knockdown (KD) of GW182, DDX6 and EDC3, another PB component (68) and SG nucleating protein TIA1 as controls in HeLa cells to examine a possible role of PB in SG biogenesis (Figure 3, Supplementary Figure S3). Western blot confirmed the KD efficiency of GW182 by ~76%, DDX6 by ~77%, EDC3 by ~81% and TIA1 by ~53% when compared to the cells treated with siNT (Figure 3A, Supplementary Figure S3B). As expected, KD of GW182 or DDX6 prevented PB formation in the HeLa cells in the absence of ARS stress as we previously reported (12) (Figure 3B, Supplementary Figure S3A), but KD of EDC3 and TIA1 did not (Supplementary Figure S3A). Consistently, EDC3 which is not required for PB formation was reported in a previous study (8). However, when the cells with the KD of individual gene expression for 48 h were exposed to ARS (0.5 mM) for 30 min to induce SG marked by G3BP1 staining, the siRNA-treated cells under ARS stress displayed an increased number of small PB by DDX6 staining if GW182 was knocked down or by GW182 staining if DDX6 was knocked down, along with overlapped SG by G3BP1 staining (Figure 3B and C bar graph for siGW182, Supplementary Table S4, Supplementary Figure S4). As expected, DCP1A staining in the cells under ARS stress displayed only partial overlapping PB staining with GW182 (Supplementary Figure S4). We also found that the cells with EDC3 KD or TIA1 KD under ARS stress had no effect, as anticipated, on PB number or shape by GW182 staining, but ~50% of TIA1 KD, not EDC3 KD, exhibited reduced formation of SG and induction of irregular SG (Supplementary Figure S4).

The unexpected increase of small PB induced by ARS in the GW182 KD cells to ~48 PB/cell, was significantly higher than that in the siNT control cells with only ~36 PB/cell (Figure 3C, Supplementary Table S4). The ARS-induced increase in PB number per cell after GW182 KD was associated with the reduction in PB size (Figure 3D, Supplementary Table S4). While GW182 KD did not significantly affect SG number per cell (Figure 3E), it significantly reduced SG size (volume) over the size in the siNT

control cells (Figure 3F, Supplementary Table S4). Interestingly, the majority of detected SG in the cells with GW182 KD were no longer topologically associated with PB (Figure 3B, Supplementary Table S1).

Like GW182, DDX6 is also essential for the formation of typical PB in the absence of stress (Figure 3B, Supplementary Figure S3). HeLa cells with DDX6 KD, in contrast to GW182 KD, exhibited a modest but significant increase of SG number per cell (Figure 3E, Supplementary Table S4) associated with reduction of SG size when compared to the siNT control cells (Figure 3F). Interestingly, compared to mostly spherical SG in the siNT control cells, many irregular SG were found in the DDX6 KD cells (Figure 3B, Supplementary Figures S4–S6). Loss of DDX6 also led to accumulation of GW182-positive PB in large clusters overlapping with SG, thus forming a hybrid PB/SG structure (Figure 3B, Supplementary Figures S4, S5, and S6). Signal distribution and intensity analyses confirmed the altered distribution of PB components in SG after DDX6 KD in HeLa cells, where GW182 and G3BP1 signals were significantly overlapped within the detected hybrid PB/SG granules (Figure 4A). These hybrid PB/SG structures feature clusters with multiple GW182-positive PB within individual SG when either the automatic background or absolute signal intensity ≥ 700 (but less than 900) threshold setting was applied (Figure 4B). Because of this feature, the Imaris image program was unable to distinguish individual GW182-positive PB in each SG-associated PB cluster, which prevents us to accurately determine the PB number and volume per DDX6 KD cell (see Figure 3B–D). However, the individual PB within each PB cluster could be counted manually for each SG (Figure 4). We found that each control siNT-treated HeLa cell under ARS stress exhibited ~6–7 large SG associated with ~2 PB, but the cells lacking DDX6 displayed ~9–10 large SG and ~11 PB within each SG-associated PB cluster (Supplementary Table S1).

Together our data show that, besides their roles in PB formation, both GW182 and DDX6 in the cells under stress are repurposed for SG biogenesis. GW182 promotes SG growth (Figure 3F) while DDX6 is to separate PB from SG during stress (Figure 4, Supplementary Figures S5 and S6). Given the potential functional overlaps between GW182 and its paralogues (12,75), we further focused on DDX6 and its role in SG biogenesis.

DDX6 is essential for the separation of PB from SG during ARS-induced stress

To avoid potential off-target effect and incomplete knockdown by siRNA approach, we employed HAP1 DDX6 knockout (DDX6KO) cells for further studies. A CRISPR/Cas9-generated 1-bp insertion in DDX6 exon 2 was used to introduce DDX6 ORF frameshift. The complete loss of DDX6 expression in HAP1 DDX6KO cells was confirmed by Western blot (Figure 5A). Loss of DDX6 expression was associated with minor morphological changes and slower growth of the cells (Figure 5B). Based on GW182 staining, HAP1 WT cells under normal physiological conditions (no ARS stress) display, on average, ~6 typical PB/cell (Figure 5C and D). Under ARS-induced stress condition, the PB number in HAP1

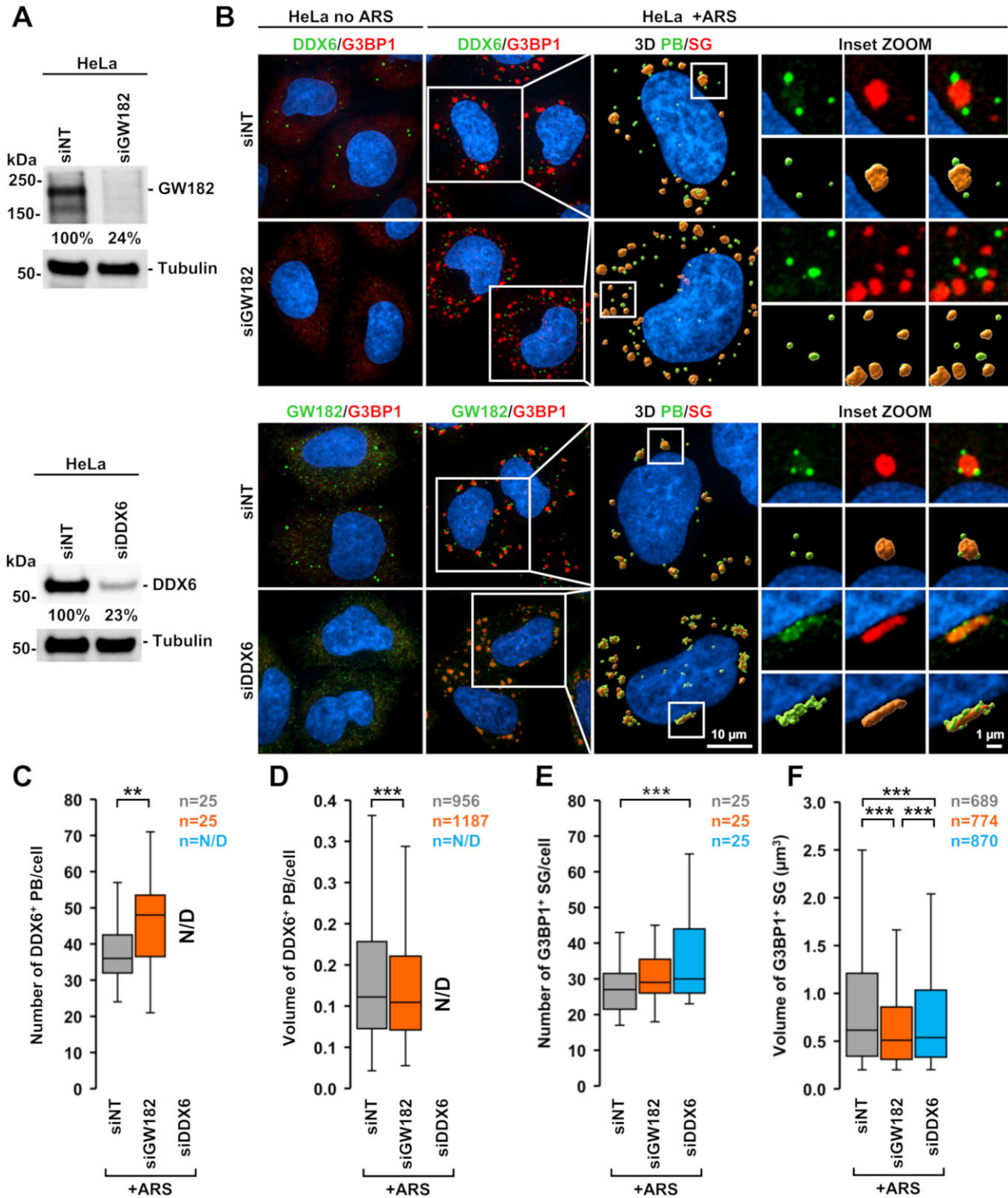


Figure 3. GW182 and DDX6 play direct roles in SG biogenesis. (A, B) HeLa cells were transfected with a non-targeting (siNT), GW182 (siGW182) or DDX6 (siDDX6) targeting siRNA. The knockdown efficiency of individual proteins was confirmed by Western blot (A). The siRNA-treated cells without (-ARS) or with (+ARS) treatment (0.5 mM, 30 min) were stained with anti-DDX6 for PB if GW182 was knocked down or anti-GW182 for PB if DDX6 was knocked down and anti-G3BP1 antibodies for SG (B). (C, F) Numbers per cell (C, E) and volume (D, F) of PB (C, D) and SG (E, F) were determined in 25 randomly selected cells in each group shown in (B). All box plots show the median (-), minimum and maximum (whiskers). *** $P < 0.001$, ** $P < 0.01$, * $P < 0.05$ by Student *t*-test; N/D: not determined.

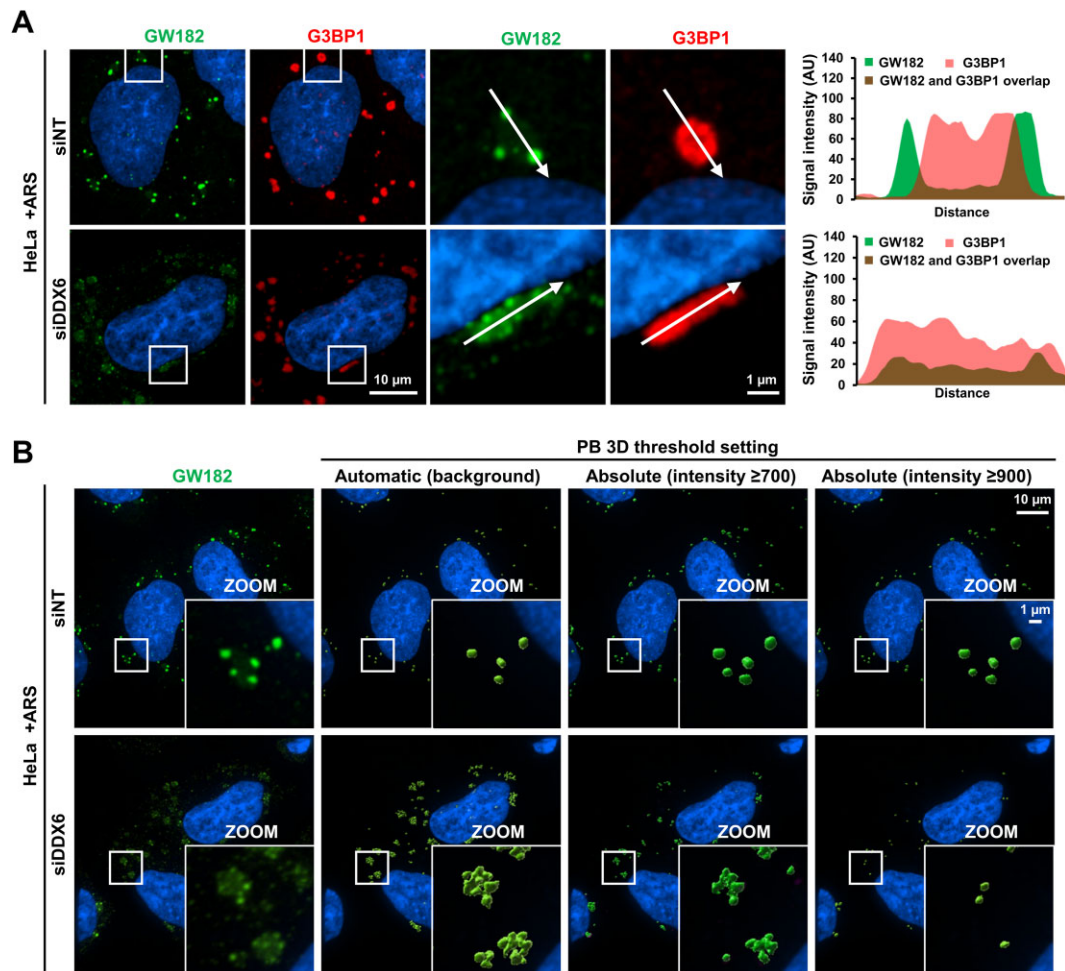


Figure 4. DDX6 knockdown led to cluster PB together and alter SG morphology in HeLa cells under ARS stress. (A) HeLa cells treated twice with non-targeting (siNT) or DDX6-targeting (siDDX6) siRNA were induced for SG formation by 0.5 mM sodium arsenite (+ARS) for 30 min before staining with GW182 for PB and G3BP1 for SG (see Figure 3B for details). The signal intensity of individual channels across the selected regions (arrows in the left panels) was determined by ImageJ and plotted in Excel (right panels). (B) Effect of various thresholds settings on PB size and number of 3D models was determined by the surface function of Imaris image analysis software based on GW182 staining.

WT cells could be increased, as observed in HeLa, to ~ 14 PB/cell (Figure 5C and D, Supplementary Table S5). ARS-treated WT HAP1 cells also exhibited ~ 8 SG/cell often associated with ~ 1 – 2 PB as observed in HeLa cells (Figure 5C and F, Supplementary Tables S1 and S5).

As expected, HAP1 DDX6KO cells do not exhibit typical PB, but rather a sand-like cytoplasmic distribution of GW182 under physiological conditions (Figure 5C and D). Interestingly, as previously observed in HeLa DDX6 KD cells (Figures 3B and 4A), we observed that DDX6KO cells under ARS stress also exhibited clustering GW182-positive granules using automatic background threshold (Figure 5C, Supplementary Figure S7). These structures represent the hybrid PB/SG granules overlapping with both PB and SG markers (Figure 5C and Supplementary Figure S7A) and prevent us to determine the PB number and volume by using Imaris image analysis software (Figure 5D and E). The GW182 mean signal intensity in G3BP1-positive SG in the DDX6KO cells under ARS stress was ~ 1.7 -fold higher than that in the SG detected in the WT cells (Figure 5G, Supplementary Figure S7A). In HeLa cells, the loss of DDX6 led

to an increase of SG number under ARS stress (Figure 3E, Supplementary Figure S5B), whereas DDX6KO in HAP1 cells under ARS stress slightly reduced SG number to ~ 6 SG/cell (Figure 5F), indicating a cell type-specific effect. Again, like in HeLa DDX6KD, the irregular SG were found in HAP1 DDX6KO cells and these irregular SG were topologically associated with a cluster of ~ 7 PB/SG (Figure 5C, Supplementary Figure S7, Supplementary Table S1), implying more GW182-positive PB and GW182 protein is presumably needed or reprogrammed in generation of ARS-induced SG when cells lack DDX6. Together, DDX6KO in HAP1 cells recapitulated the results observed in HeLa cells, confirming the essential role of DDX6 in the separation of PB and SG during ARS-induced stress.

Separation of PB from SG requires DDX6 helicase activity

By remodeling RNP complexes, DEAD-box RNA helicases play essential roles in many biological processes (76). They also possess ATPase activity required for their helicase activity. Although DDX6 helicase activity is

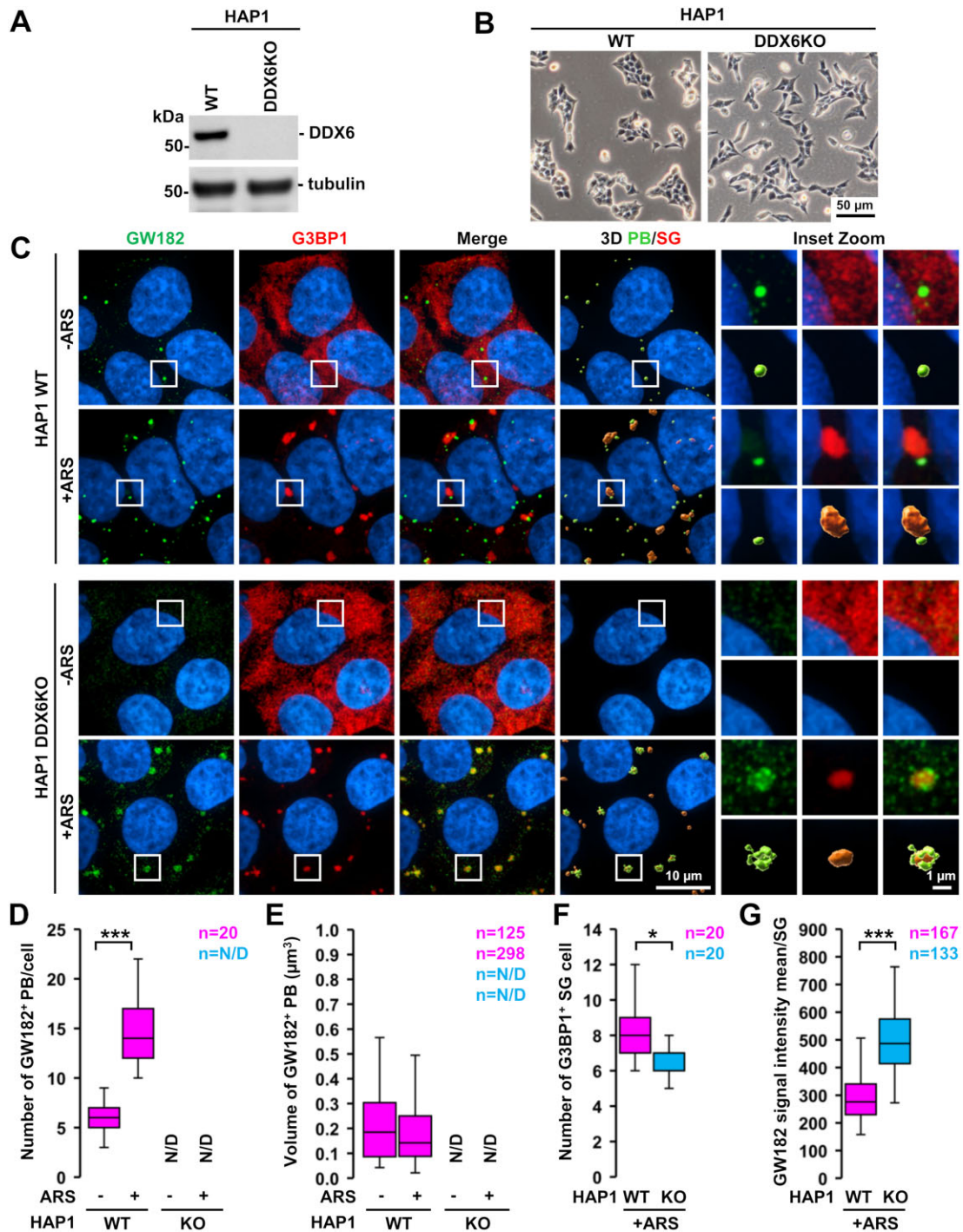


Figure 5. DDX6 is required for separation of PB from SG during ARS stress. (A) Western blot analysis of DDX6 protein expression in HAP1 wild-type (WT) and DDX6 knockout (DDX6KO) cells. Cellular tubulin served as a loading control. (B) Morphology of the WT and DDX6KO HAP1 cells as detected by light microscopy of living cells. (C) Immunofluorescent staining of the HAP1 WT and DDX6KO cells without (-ARS) or with (+ARS) arsenite treatment (0.5 mM, 30 min) using GW182 as a marker for PB and G3BP1 for SG. (D-F) Numbers per cell (D, F) and volume (E) of PB (D, E) and SG (F) in the WT and DDX6 KO cells based on 20 randomly selected cells in each group. (G) The mean GW182 signal intensity in all SG detected in the WT or DDX6KO cells. All box plots show the median (-), minimum and maximum (whiskers). *** $P < 0.001$, ** $P < 0.01$, * $P < 0.05$ by Student's *t*-test; N/D: not determined.

essential for *de novo* PB assembly under physiological conditions (19), other studies have suggested that DDX6 RNA helicase activity had no effect on preexisting PB (19,71,77). To test the importance of DDX6 helicase activity in SG biogenesis and whether it is essential for separating PB from SG in the cells under ARS stress, we disrupted DDX6 helicase activity by converting glutamic acid residue at amino acid position 247 to alanine (E247A) in DDX6 DEAD-box motif (Figure 6A). Structural modeling based on similarities to other DEAD-box helicases, such as the DDX3X (72) and Ski2-like RNA-helicase Brr2 (73), indicated that E247 in DDX6 is important in mediating ATP-binding and hydrolysis that is needed for DDX6 function (Figure 6B). The constructed expression vectors encoding DDX6 wild-type (WT) or helicase-deficient E247A mutant contain the epitope tags (myc-FLAG) allowing specific detection of the ectopically expressed DDX6, distinguishable from the endogenous cellular DDX6 (Figure 6A). To test how inactivation of helicase activity affects DDX6 function, we rescued DDX6 expression in HAP1 DDX6KO cells by transfecting either the WT or the helicase deficient E247A mutant (Figure 6C). Under physiological conditions, expression of the WT DDX6 led to the formation of DDX6-positive granules resembling typical PB, which was confirmed by GW182 staining (Figure 6C, -ARS). Upon ARS treatment, the cells rescued with the WT DDX6 formed DDX6-positive PB together with typical G3BP1-positive SG (Figure 6C, +ARS). The typical PB and SG were often spatially linked but distinct from each other as observed in the WT cells (Figure 5C). In contrast, expression of the E247A mutant DDX6 in the DDX6KO cells failed to restore PB formation under physiological conditions, with the mutant DDX6 consistently exhibiting diffused cytoplasmic staining of the PB markers (Figure 6C, -ARS). After ARS treatment, the E247A DDX6 mutant accumulated in many extended, irregularly shaped granules double positive for PB (GW182) and SG (G3BP1) markers (Figure 6C, +ARS), thus resembling the hybrid PB/SG granules also observed in HeLa DDX6 KD (Figure 3B, +ARS, Figure 4, Supplementary Figures S5 and S6) and HAP1 DDX6KO cells (Figure 5C, +ARS). The same activities of DDX6 WT and E247A mutant were observed in the rescue of DDX6 expression on SG biogenesis in HeLa DDX6 KD cells under ARS stress (Supplementary Figure S8).

DDX6 activity is modulated by its interacting partners

Besides binding to RNA, DDX6 also binds numerous protein factors primarily through its RecA2 domain (Figure 6A) (8,78). Many of these interactions are mutually exclusive, allowing the formation of distinct DDX6 complexes (67). To examine whether DDX6-interactions are functionally required for the DDX6's role in SG biogenesis, we knocked down the expression of previously identified DDX6-interacting partners PATL1 (PB associated mRNA decay factor), CNOT1 (CCR4-NOT transcription complex subunit 1), and 4E-T (EIF4ENIF1, eukaryotic translation initiation factor 4E nuclear import factor 1) in HeLa cells using gene-specific siRNAs (Figure 7A). The numbers of PB and SG were determined by GW182 and G3BP1 staining, respectively, in the cells without or with ARS treat-

ment. Consistent with previous reports (8,78), PATL1 was not essential for PB formation under normal physiological conditions (Supplementary Figure S3, no ARS). Under ARS stress, PATL1 KD led only to a slight reduction of PB number but not volume compared to siNT control cells (Figure 7B–D, Supplementary Table S6). The KD of CNOT1 in HeLa cells in stress free condition (no ARS) displayed no effect on PB formation (Supplementary Figure S3C), which is different from a reported study by using AGO2-GFP reporter assay (79). However, during ARS stress the loss of CNOT1 was associated with formation of PB clusters closely resembling those observed in cells lacking DDX6 (Figure 7B). As reported (8,46,67,80), 4E-T was also essential for PB formation and KD of 4E-T in HeLa cells led to block PB formation in the absence of ARS stress (Supplementary Figure S3C). In contrast, ARS treatment of the 4E-T KD cells resulted in formation of ~87 PB/cell that were almost three times of ~31 PB/cell observed in the siNT control cells (Figure 7B and C, Supplementary Table S6). PB in the 4E-T KD cells were significantly smaller (Figure 7D) and mostly tightly associated with the newly formed SG positive for G3BP1 staining (Figure 7B).

Knockdown of any of the tested DDX6 co-factors in HeLa cells did not significantly affect SG number or volume when compared to the siNT control cells (Figure 7E and F, Supplementary Table S6). However, knockdown of either CNOT1 or 4E-T was associated with altered SG morphology characterized by the formation of extended irregularly shaped SG linked with clustered PB stained by GW182 (Figure 7B), thus to various extent resembling the hybrid PB/SG granules in HeLa DDX6 KD cells (Figure 3B, +ARS, Figure 4, Supplementary Figures S5 and S6). The manual count of GW182-positive PB in the PB clusters within each SG in the HeLa cells with KD of CNOT1 or 4E-T under ARS stress exhibited ~8–9 PB/SG, that is also similar to ~11 PB/SG observed in HeLa DDX6 KD cells. In comparison, the control siNT-treated cells and PATL1 KD cells exhibited only ~2 PB/SG as observed in the cells without siRNA treatment (Supplementary Table S1). Interestingly in all cases, DDX6 showed close colocalization with GW182 staining both in the siNT-treated control and gene-specific knockdown cells (Supplementary Figure S9). On the contrary, DCP1A only partially overlapped with GW182-positive granules in control and siPATL1-treated cells and was mainly excluded from GW182-granules in siCNOT1- and si4E-T-treated cells (Supplementary Figure S10). All together, these results indicate that proper PB and SG separation also depends on DDX6 interacting partners CNOT1 and 4E-T that presumably act by modulation of DDX6 helicase/ATPase activity as previously shown (81).

GW182 acts independently of DDX6 in SG biogenesis

To investigate if the activity of above-mentioned PB components in SG biogenesis depends on their binding to DDX6, we knocked down GW182, CNOT1, and 4E-T, separately, in HAP1 WT and DDX6KO cells (Figure 8A). The cells treated with non-targeting (siNT) siRNA served as a negative control. After knockdown, the cells were treated with ARS for 30 min to induce SG and stained with anti-LSM14A, a true PB marker separately from GW182 for PB

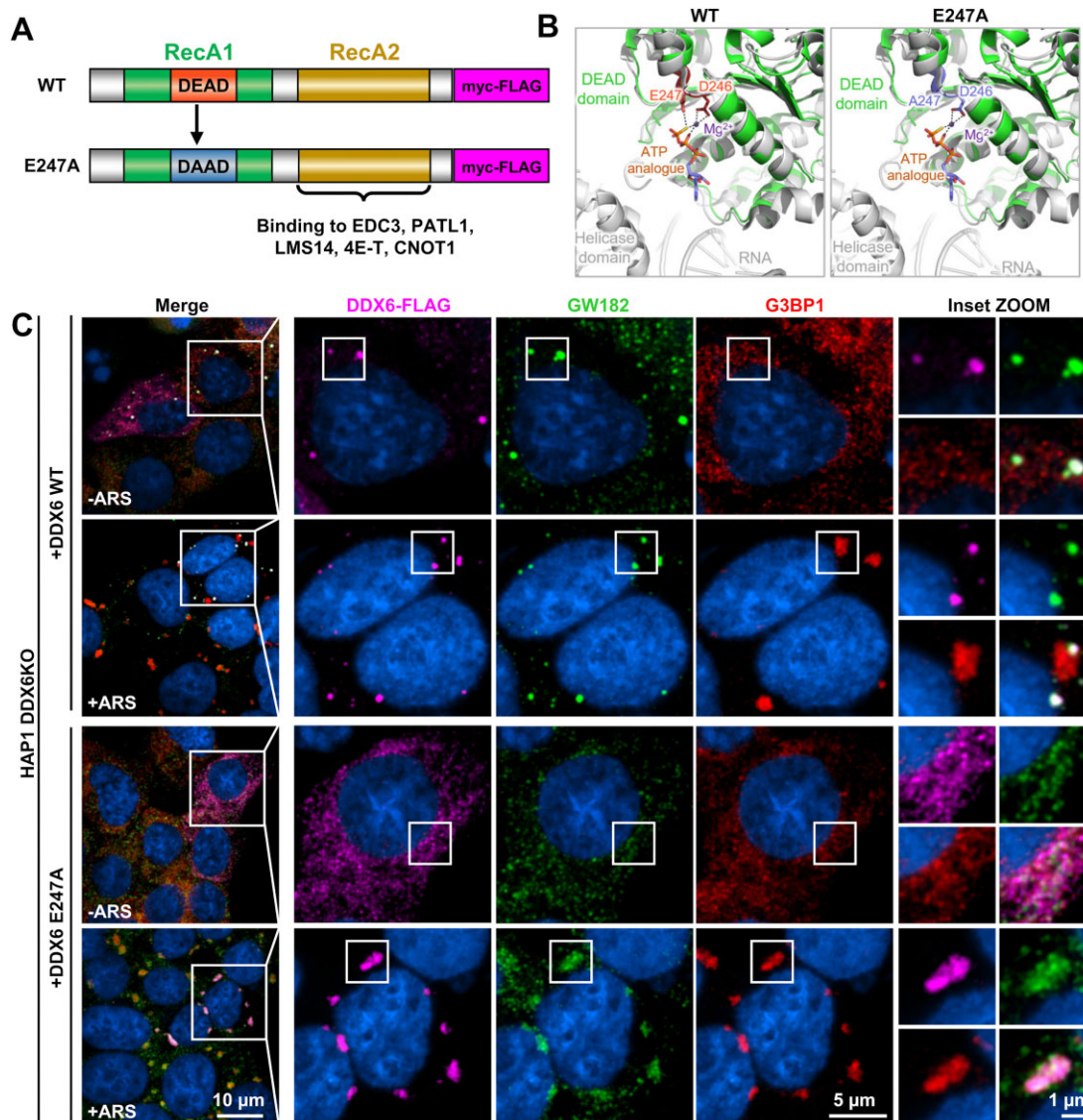


Figure 6. DDX6 helicase activity is essential for separation of PB from SG. (A) A diagram of ectopically expressed wild type (WT) human DDX6 with two RecA-like domains (RecA1, green, RecA2, yellow). The DEAD-box motif located in the RecA1 is shown in the red box. The helicase deficient E247A mutant is shown below with a mutated DAAD-box in the blue box. Both proteins were fused with c-myc and FLAG tags on the C-terminus. Proteins binding to the DDX6 C-terminal RecA2 domain (8,78) are shown below. (B) Predicted structural consequences for the E247A mutation. The DEAD-box motif of DDX6 (PDB ID: 5ANR, green cartoon) is superposed with the DEAD-box of RNA helicase DDX3X at the pre-unwound state (PDB ID: 6O5F, gray cartoon) to show the relative locations of DEAD-box and helicase domain. An ATP analog (ATP- γ -S) and an Mg²⁺ critical for ATP hydrolysis are modeled based on alignment with the Ski2 RNA-helicase Brr2 (PDB ID: 6QV4). The DEAD-box motif in the wild type (WT) and E247A mutant DDX6 are shown in pink and blue, respectively, with the D246 and E247A residues in stick representation. Bonds between D246, E247, ATP- γ -S and Mg²⁺ are shown in dash lines. The E247A mutation abolishes critical chemical interactions needed for ATP binding and/or hydrolysis. (C) HAP1 DDX6KO cells were transfected with a vector expressing myc-FLAG-tagged wild type (WT) or helicase-deficient (E247A) DDX6 mutant. Twenty-four hours after transfection, the cells were incubated in the absence (-ARS) or presence (+ARS) of 0.5 mM arsenite for 30 min before immunofluorescent staining with an anti-FLAG antibody to detect ectopically expressed DDX6, anti-GW182 for PB and anti-G3BP1 for SG.

(Supplementary Figure S11) as described (82,83) and anti-G3BP1 for SG. As shown in Figure 8B and Supplementary Figure S11, the WT cells without (Supplementary Figures S11C) or with siNT treatment (Figure 8B) formed typical LSM14A⁺ PB and G3BP1⁺ SG in response to ARS, with large SG formed in the proximity of LSM14A⁺ PB. Again, number of DCP1A-positive PB was much less than that of LSM14A-positive PB in the ARS-stressed cells (compare the Supplementary Figure S11D to S11C). Interestingly,

KD of GW182, CNOT1 or 4E-T in HAP1 DDX6WT cells significantly increased SG number (Figure 8D) without affecting SG volume (Figure 8E, Supplementary Table S7). It is noticeable that most of the SG in the HAP1 cells with KD of CNOT1 or 4E-T, but not with the GW182 KD, were the hybrid PB/SG hybrid granules (Figure 8B) with the irregular shape and associated with PB clusters as observed in DDX6-deficient cells (Figure 5C and Supplementary Figure S7). By manual count of PB number in the cluster in

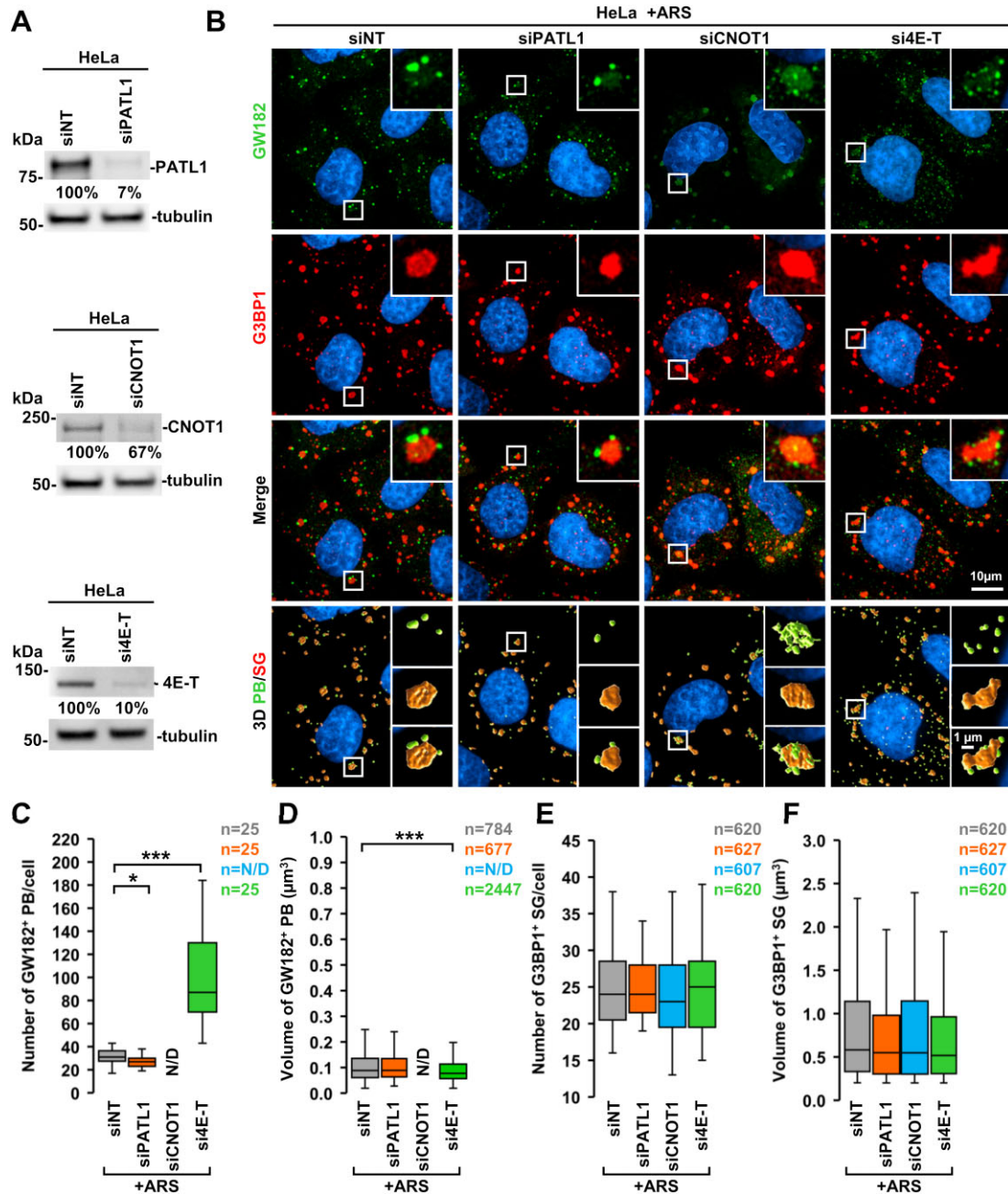


Figure 7. Modulation of DDX6 activity in PB and SG biogenesis by its interacting partners. (A, B) HeLa cells were transfected either with a non-targeting siRNA (siNT) or siRNA targeting DDX6 interactors PATL1 (siPATL1), CNOT1 (siCNOT1), or 4E-T (si4E-T). The efficiency of siRNA-induced knockdown of individual proteins was determined by western blot (A). The effect of individual protein knockdown on PB and SG formation in cells without (-ARS) or with (+ARS) arsenite treatment (0.5 mM, 30 min) was determined by immunofluorescent staining with GW182 for PB and G3BP1 for SG (B). (C–F) Numbers per cell (C, E) and volume (D, F) of PB (C–D) and SG (E, F) were determined in 25 randomly chosen cells from each group shown in the panel B. All box plots show the median (–), minimum and maximum (whiskers). *** $P < 0.001$, ** $P < 0.01$, * $P < 0.05$ by Student's *t*-test; N/D: not determined.

each SG, we found that HAP1 cells with KD of CNOT1 or 4E-T under ARS stress exhibited, ~6–7 PB/SG, when compared with the ~1 PB/SG in control (siNT) or GW182 KD cells at the same condition (Supplementary Table S1). Data suggest GW182 functions differently from CNOT1 and 4E-T in regulation of SG formation in HAP1 cells.

Since CNOT1 and 4E-T interact directly with DDX6 via binding to its C-terminal RecA2 domain (Figure 6A),

we next examined if their activity is dependent on DDX6 and how their knockdown affects SG formation in HAP1 DDX6KO cells (Figure 8C). As previously observed in Figure 5C, due to the lack of DDX6 separation activity, the control siNT-treated DDX6KO cells form only the hybrid PB/SG granules in the presence of ARS stress (Figure 8C). Interestingly, GW182 retained its activity in the DDX6KO cells with GW182KD leading to the formation of more and

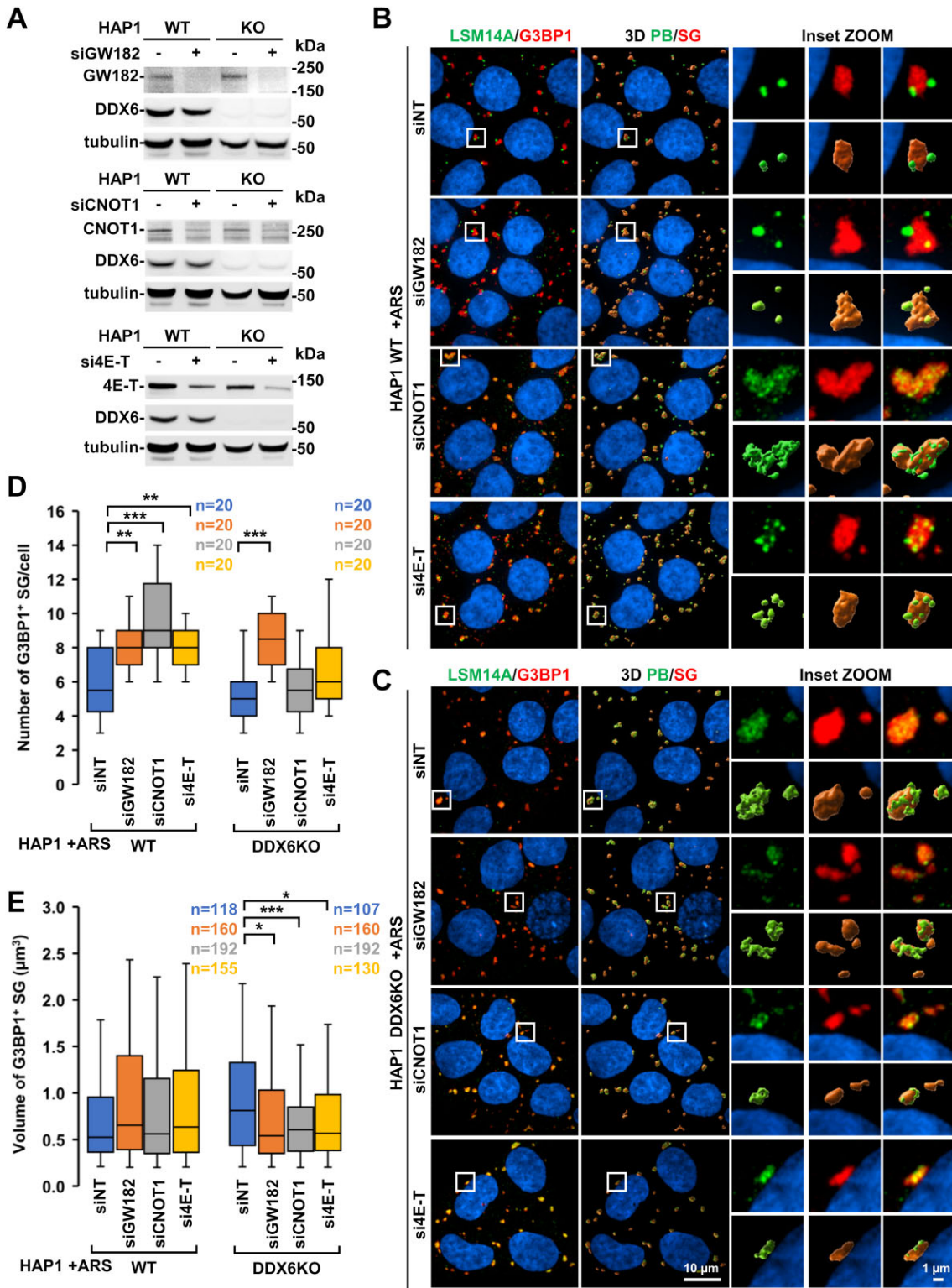


Figure 8. DDX6 interacting factors in DDX6-mediated SG biogenesis. HAP1 wild type (WT) and DDX6 knockout (DDX6KO) cells were transfected with non-targeting (siNT) or siRNA targeting GW182 (siGW182), CNOT1 (siCNOT1), and 4E-T (si4E-T). The siRNA-mediated knockdown efficiency was determined by Western blot (A). (B, C) The siRNA-treated cells were treated with 0.5 mM arsenite (+ARS) for 30 min and stained with an anti-LSM14A antibody for PB and anti-G3BP1 antibody for SG, which are shown in fluorescent and 3D images. Numbers (D) and volume (E) of SG per cell were calculated from 20 randomly selected HAP1 WT or DDX6KO cells treated with a non-targeting (siNT) or gene-specific siRNAs. The box blot shows the median (–), minimum and maximum (whiskers). *** $P < 0.001$, ** $P < 0.01$, * $P < 0.05$ by Student's *t*-test.

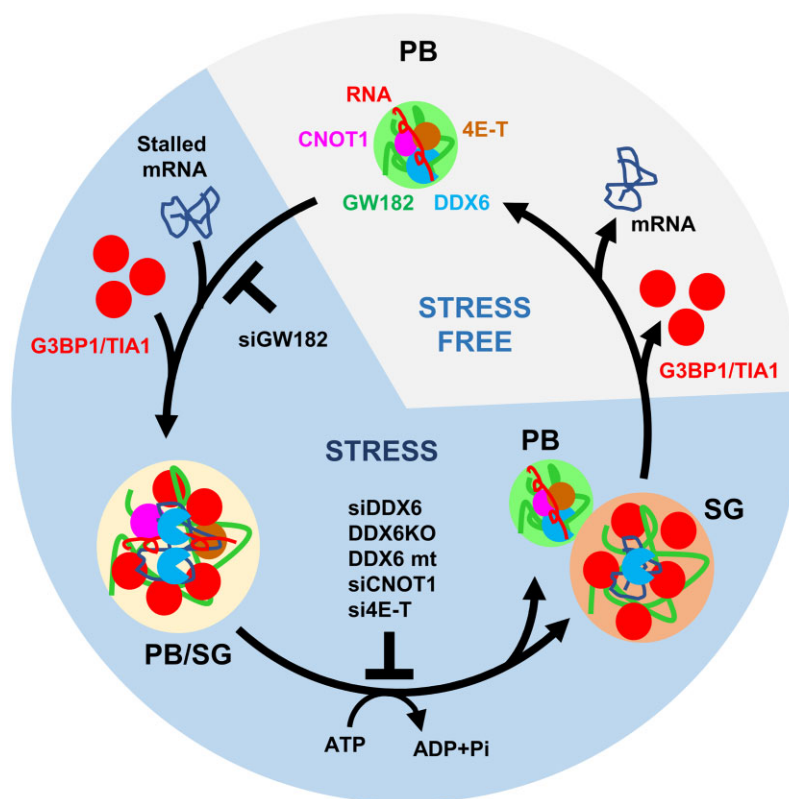


Figure 9. The proposed model of distinct roles of PB components in SG biogenesis. An integrated model of how PB contribute to SG biogenesis during cellular stress, where GW182 acts as a scaffold for recruiting the stalled mRNA in interaction with TIA1 and G3BP1 and promotes assembly of mature SG via hybrid PB/SG bodies followed by DDX6-mediated separation of PB from SG components. This separation depends on DDX6 helicase/ATPase activities which could be modulated by DDX6 interacting partners CNOT1 and 4E-T. Thus, knockdown by individual siRNAs or deletion or mutation of these factors will severely interrupt PB-mediated SG biogenesis and separation of PB from SG. Stress relief makes SG collapse and the cells back to a normal condition with cells bearing PB for storage of viable RNAs useful for incoming cell proliferation and cycling.

significantly smaller SG when compared to control siNT-treated cells (Figure 8C–E, Supplementary Table S7). Opposite to WT HAP1 cells, knockdown of CNOT1 and 4E-T in HAP1 DDX6KO cells had no significant effect on SG numbers while only significantly reducing SG size (Figure 8C–E, Supplementary Table S7). In all cases the DDX6KO cells exhibited irregular hybrid PB/SG granules, indicating that KD of any tested factor cannot relieve or rescue the loss of DDX6 separation activity, and thus, the number of PB per SG or per PB cluster remained unchanged (~6–7 PB/SG) in all HAP1 DDX6KO cells (Supplementary Table S1). In summary, our data also argue for the first time for distinct activities of individual DDX6 interactors in SG biogenesis. While the scaffolding activity of GW182 repurposed in ARS stress for HAP1 cells to increase PB and SG number is independent of DDX6, DDX6 is indispensable for separation of PB from SG during ARS stress and its activity could be modulated by its interacting partners CNOT1 and 4E-T, but not GW182.

DISCUSSION

Many groups have investigated the formation, regulation, and function of PB and SG, but the intimate biomolecular relationship between them remains mysterious. Here, we describe the dependence of SG biogenesis selectively on

PB components under ARS stress and uncover the direct roles of PB components in SG biogenesis. As summarized in the proposed model (Figure 9), we found that GW182 undertaking a general scaffold activity and DDX6 carrying helicase activity are necessary for PB *de novo* assembly as well as SG biogenesis under ARS stress. DDX6 also promotes the separation of PB from SG. This separation activity of DDX6 is modulated by two DDX6-interacting proteins, CNOT1 and 4E-T, which presumably regulate DDX6 helicase activity by binding to the DDX6 RecA2 domain.

Our observations demonstrated that SG are topologically and mechanically linked to PB in the cells under ARS stress, where major PB components GW182, DDX6, and LSM14A are significantly overlapped with SG. A striking discovery in our study is the observation of the stress-induced hybrid PB/SG granules in both HeLa and HAP1 cells lacking DDX6 helicase or its interacting protein CNOT1 and 4E-T. These hybrid PB/SG granules are featured by a GW182- or LSM14A-positive PB cluster on each SG and the multiple PB in the cluster surround a newly formed SG. We interpret that formation of the hybrid granules in the absence of DDX6 helicase activity might represent a previously unknown, intermediate transition step from PB to SG in a rapid cellular response to a large amount of influx RNA released from polysomes during ARS stress (Figure 9), that are resulted from condensation of

nonselective heterogeneous macromolecules of PB and SG components (52,55). The following ‘demixing’ into distinct PB and SG is a selective, energy-dependent process requiring DDX6 helicase activity and its interacting proteins (Figure 9). The finding that nearly half (62/125) of PB proteins are associated with DDX6 (3,8) might provide a source of such selectivity. Thus, our work provides a sensible mechanistic model (Figure 9) for the observed intimate interconnection between PB and SG.

In the cells with DDX6 helicase activity, we found that SG are formed in a stepwise process by aggregation or repurposing of preexisting PB components and SG nucleating factors in a time-dependent manner. This coalescence occurs topologically in proximity to PB. As a result, almost every SG has at least one associated PB (~1PB at 15 min to ~2–3 PB at 30 min). Interestingly, the number of stress-induced SG was always fewer than the number of PB. Thus, not every PB in the cells under stress is associated with SG. As previous reports (8), we found that ARS stress also induces PB formation and thus increases PB quantity in the cells no matter which PB marker was used for staining. One can argue for a passive accumulation of PB components within SG due to elevated number of PB in the vicinity of where large SG are formed. However, our observation that selective accumulation GW182, DDX6, and LSM14A, but not DCP1A, in SG suggests a rather active recruitment of these factors in SG biogenesis during ARS stress. DCP1A presents only in a subset of PB and is dispensable for PB biogenesis (9,12).

We found that GW182 progressively accumulates in SG as a scaffold protein to facilitate SG ‘growth’ because lack of GW182 led to a reduction in SG size and their topological dissociation from PB in HeLa cells. This is compatible with a proposed structure of ‘mature = large’ SG consisting of rigid ‘cores’ enriched in SG markers surrounded by heterogeneous and dynamic ‘shell’ (84,85). The observed GW182 scaffolding activities in PB formation (12,86) is also supported by its long intrinsically disordered regions with high binding potentials (<https://alphafold.ebi.ac.uk/entry/Q8NDV7>), which provides a plausible molecular mechanism in stress-induced GW182 reprogramming for SG nucleation possibly by cooperation with other known SG nucleation factors (55,85). However, it remains unclear what functions of other two human GW182 paralogues, TNRC6A-1, and TNRC6B-1, in SG biogenesis are and our study in this report only focused on GW182 TNRC6A-2 (12,75). As deletion of individual TNRC6 promotes the compensatory expression of remaining members (75), it may contribute to varied phenotypic SG size from one cell type to another under ARS stress. We noticed that the effect of GW182 KD on ARS-induced SG size differs from HeLa to HAP1 cells.

We found that the major function of DDX6 is to separate PB from SG during ARS stress, although the dependency of PB formation on DDX6 in both physiological and stress conditions are well documented from yeast to mammalian cells (8,12,50). The cells lacking DDX6 under ARS stress form irregular SG granules surrounded by a cluster of multiple PB. DDX6KO cells can be rescued by exogenous DDX6 to separate PB from SG. This lack of built-in redundancy, typical for many cellular processes, is surpris-

ing, because both PB and SG are enriched in several other RNA-helicases, including UPF1, MOV10, eIF4A (DDX2), DDX3, and RNA helicase A (DHX9) (3,4,57,58). Despite of high abundance, only ~10% of total DDX6 appear to be localized in PB (65). Besides its RNA-binding and helicase activity, DDX6 interacts with many proteins through its RecA2 domain (8,19,68), which are often mutually exclusive and have opposite effect on DDX6 activity (68,77,87). We observed that DDX6 interactors PALT1 and CNOT1 are dispensable for PB formation in the absence of ARS stress, as reported (8,78). CNOT1 and 4E-T knockdowns induces the hybrid PB/SG granules in the cells containing a functional DDX6. This phenotypical similarity between knockdowns of DDX6, CNOT1, and 4E-T in induction of the hybrid PB/SG granules could be explained by CNOT1 stimulation of DDX6 ATPase activity (78). 4E-T binding DDX6 RecA2 domain via a different binding site from CNOT1 may possess the similar stimulatory activity (67,78). In contrast, CNOT1 and PATL1 binding to DDX6 are mutually exclusive as they share the same binding motif also used for EDC3 and LSM14A binding (68). The high sequence and functional conservation of DDX6 from yeast to human and rare human polymorphism further supports its essential role in basic cell biology (88).

In summary, our discovery in this report that the direct roles of two major PB components, GW182 and DDX6, play in SG biogenesis represents a significant conceptual shift in our understanding of PB and SG biology. Our findings provide a mechanistic interpretation of the intimate interconnection from PB to SG. Most importantly, it emphasizes the roles of PB components in regulating gene expression in cells not only under physiological condition but also under stress.

DATA AVAILABILITY

The data underlying this article are available in the article and in its online supplementary material.

SUPPLEMENTARY DATA

Supplementary Data are available at NAR Online.

ACKNOWLEDGEMENTS

We thank Dr. Marvin Fritzler of the University of Calgary for kindly providing us the autoimmune serum for GW182 staining. We would also gratefully acknowledge the Optical Microscopy and Analysis Laboratory of the Frederick National Laboratory for Cancer Research for their scientific support.

FUNDING

Center for Cancer Research, National Cancer Institute, National Institutes of Health, Intramural Research Program [ZIA5010357 to Z.M.Z.]. Funding for open access charge: Center for Cancer Research, National Cancer Institute, National Institutes of Health.

Conflict of interest statement. None declared.

REFERENCES

- Riggs, C.L., Kedersha, N., Ivanov, P. and Anderson, P. (2020) Mammalian stress granules and P bodies at a glance. *J. Cell Sci.*, **133**, jcs.242487.
- Kedersha, N. and Anderson, P. (2007) Mammalian stress granules and processing bodies. *Methods Enzymol.*, **431**, 61–81.
- Hubstenberger, A., Courel, M., Bénard, M., Souquere, S., Ernoult-Lange, M., Chouaib, R., Yi, Z., Morlot, J.B., Munier, A., Fradet, M. et al. (2017) P-body purification reveals the condensation of repressed mRNA regulons. *Mol. Cell*, **68**, 144–157.
- Youn, J.Y., Dunham, W.H., Hong, S.J., Knight, J.D.R., Bashkurov, M., Chen, G.I., Bagci, H., Rathod, B., MacLeod, G., Eng, S.W.M. et al. (2018) High-density proximity mapping reveals the subcellular organization of mRNA-associated granules and bodies. *Mol. Cell*, **69**, 517–532.
- Cougot, N., Babajko, S. and Séraphin, B. (2004) Cytoplasmic foci are sites of mRNA decay in human cells. *J. Cell Biol.*, **165**, 31–40.
- Liu, J., Valencia-Sanchez, M.A., Hannon, G.J. and Parker, R. (2005) MicroRNA-dependent localization of targeted mRNAs to mammalian P-bodies. *Nat. Cell Biol.*, **7**, 719–723.
- Sheth, U. and Parker, R. (2003) Decapping and decay of messenger RNA occur in cytoplasmic processing bodies. *Science*, **300**, 805–808.
- Ayache, J., Bénard, M., Ernoult-Lange, M., Minshall, N., Standart, N., Kress, M. and Weil, D. (2015) P-body assembly requires DDX6 repression complexes rather than decay or Ataxin2/2L complexes. *Mol. Biol. Cell*, **26**, 2579–2595.
- Eulalio, A., Behm-Ansmant, I., Schweizer, D. and Izaurralde, E. (2007) P-body formation is a consequence, not the cause, of RNA-mediated gene silencing. *Mol. Cell Biol.*, **27**, 3970–3981.
- Horvathova, I., Voigt, F., Kotrys, A.V., Zhan, Y., Artus-Revel, C.G., Eglinger, J., Stadler, M.B., Giorgetti, L. and Chao, J.A. (2017) The dynamics of mRNA turnover revealed by single-molecule imaging in single cells. *Mol. Cell*, **68**, 615–625.
- Parker, R. and Sheth, U. (2007) P bodies and the control of mRNA translation and degradation. *Mol. Cell*, **25**, 635–646.
- Sharma, N.R., Majercki, V., Kruhlak, M.J., Yu, L., Kang, J.G., Yang, A., Gu, S., Fritzler, M.J. and Zheng, Z.M. (2019) KSHV RNA-binding protein ORF57 inhibits P-body formation to promote viral multiplication by interaction with Ago2 and GW182. *Nucleic Acids Res.*, **47**, 9368–9385.
- Courel, M., Clément, Y., Bossevain, C., Foretek, D., Vidal Cruchez, O., Yi, Z., Bénard, M., Benassy, M.N., Kress, M., Vindry, C. et al. (2019) GC content shapes mRNA storage and decay in human cells. *Elife*, **8**, e49708.
- Matheny, T., Rao, B.S. and Parker, R. (2019) Transcriptome-wide comparison of stress granules and P-bodies reveals that translation plays a major role in RNA partitioning. *Mol. Cell Biol.*, **39**, e00313-19.
- Aizer, A., Kalo, A., Kafri, P., Shraga, A., Ben-Yishay, R., Jacob, A., Kinor, N. and Shav-Tal, Y. (2014) Quantifying mRNA targeting to P-bodies in living human cells reveals their dual role in mRNA decay and storage. *J. Cell Sci.*, **127**, 4443–4456.
- Bregues, M., Teixeira, D. and Parker, R. (2005) Movement of eukaryotic mRNAs between polysomes and cytoplasmic processing bodies. *Science*, **310**, 486–489.
- Wilbertz, J.H., Voigt, F., Horvathova, I., Roth, G., Zhan, Y. and Chao, J.A. (2019) Single-molecule imaging of mRNA localization and regulation during the integrated stress response. *Mol. Cell*, **73**, 946–958.
- Kedersha, N., Tisdale, S., Hickman, T. and Anderson, P. (2008) Real-time and quantitative imaging of mammalian stress granules and processing bodies. *Methods Enzymol.*, **448**, 521–552.
- Minshall, N., Kress, M., Weil, D. and Standart, N. (2009) Role of p54 RNA helicase activity and its C-terminal domain in translational repression, P-body localization and assembly. *Mol. Biol. Cell*, **20**, 2464–2472.
- Hofmann, S., Kedersha, N., Anderson, P. and Ivanov, P. (2021) Molecular mechanisms of stress granule assembly and disassembly. *Biochim. Biophys. Acta Mol. Cell Res.*, **1868**, 118876.
- Bouedjah, O., Hamon, L., Savarin, P., Desforges, B., Curmi, P.A. and Pastré, D. (2012) Macromolecular crowding regulates assembly of mRNA stress granules after osmotic stress: new role for compatible osmolytes. *J. Biol. Chem.*, **287**, 2446–2458.
- Kedersha, N.L., Gupta, M., Li, W., Miller, I. and Anderson, P. (1999) RNA-binding proteins TIA-1 and TIAR link the phosphorylation of eIF-2 alpha to the assembly of mammalian stress granules. *J. Cell Biol.*, **147**, 1431–1442.
- Kwon, S., Zhang, Y. and Matthias, P. (2007) The deacetylase HDAC6 is a novel critical component of stress granules involved in the stress response. *Genes Dev.*, **21**, 3381–3394.
- Sharma, N.R., Majercki, V., Kruhlak, M.J. and Zheng, Z.M. (2017) KSHV inhibits stress granule formation by viral ORF57 blocking PKR activation. *PLoS Pathog.*, **13**, e1006677.
- Donnelly, N., Gorman, A.M., Gupta, S. and Samali, A. (2013) The eIF2α kinases: their structures and functions. *Cell. Mol. Life Sci.*, **70**, 3493–3511.
- Harding, H.P., Zhang, Y., Bertolotti, A., Zeng, H. and Ron, D. (2000) Perk is essential for translational regulation and cell survival during the unfolded protein response. *Mol. Cell*, **5**, 897–904.
- McEwen, E., Kedersha, N., Song, B., Scheuner, D., Gilks, N., Han, A., Chen, J.J., Anderson, P. and Kaufman, R.J. (2005) Heme-regulated inhibitor kinase-mediated phosphorylation of eukaryotic translation initiation factor 2 inhibits translation, induces stress granule formation, and mediates survival upon arsenite exposure. *J. Biol. Chem.*, **280**, 16925–16933.
- Srivastava, S.P., Kumar, K.U. and Kaufman, R.J. (1998) Phosphorylation of eukaryotic translation initiation factor 2 mediates apoptosis in response to activation of the double-stranded RNA-dependent protein kinase. *J. Biol. Chem.*, **273**, 2416–2423.
- Wek, S.A., Zhu, S. and Wek, R.C. (1995) The histidyl-tRNA synthetase-related sequence in the eIF-2 alpha protein kinase GCN2 interacts with tRNA and is required for activation in response to starvation for different amino acids. *Mol. Cell Biol.*, **15**, 4497–4506.
- Lu, J., O'Hara, E.B., Trieselmann, B.A., Romano, P.R. and Dever, T.E. (1999) The interferon-induced double-stranded RNA-activated protein kinase PKR will phosphorylate serine, threonine, or tyrosine at residue 51 in eukaryotic initiation factor 2alpha. *J. Biol. Chem.*, **274**, 32198–32203.
- Gray, N.K. and Wickens, M. (1998) Control of translation initiation in animals. *Annu. Rev. Cell Dev. Biol.*, **14**, 399–458.
- Jackson, R.J., Hellen, C.U. and Pestova, T.V. (2010) The mechanism of eukaryotic translation initiation and principles of its regulation. *Nat. Rev. Mol. Cell Biol.*, **11**, 113–127.
- Kedersha, N., Chen, S., Gilks, N., Li, W., Miller, I.J., Stahl, J. and Anderson, P. (2002) Evidence that ternary complex (eIF2-GTP-tRNA(i)(Met))-deficient preinitiation complexes are core constituents of mammalian stress granules. *Mol. Biol. Cell*, **13**, 195–210.
- Gilks, N., Kedersha, N., Ayodele, M., Shen, L., Stoecklin, G., Dember, L.M. and Anderson, P. (2004) Stress granule assembly is mediated by prion-like aggregation of TIA-1. *Mol. Biol. Cell*, **15**, 5383–5398.
- Kedersha, N., Cho, M.R., Li, W., Yacono, P.W., Chen, S., Gilks, N., Golan, D.E. and Anderson, P. (2000) Dynamic shuttling of TIA-1 accompanies the recruitment of mRNA to mammalian stress granules. *J. Cell Biol.*, **151**, 1257–1268.
- Kedersha, N., Panas, M.D., Achorn, C.A., Lyons, S., Tisdale, S., Hickman, T., Thomas, M., Lieberman, J., McInerney, G.M., Ivanov, P. et al. (2016) G3BP-Caprin1-USP10 complexes mediate stress granule condensation and associate with 40S subunits. *J. Cell Biol.*, **212**, 845–860.
- Tourrière, H., Chebli, K., Zekri, L., Courselaud, B., Blanchard, J.M., Bertrand, E. and Tazi, J. (2003) The RasGAP-associated endoribonuclease G3BP assembles stress granules. *J. Cell Biol.*, **160**, 823–831.
- Sidrauski, C., McGeachy, A.M., Ingolia, N.T. and Walter, P. (2015) The small molecule ISRIB reverses the effects of eIF2α phosphorylation on translation and stress granule assembly. *Elife*, **4**, e05033.
- Dang, Y., Kedersha, N., Low, W.K., Romo, D., Gorospe, M., Kaufman, R., Anderson, P. and Liu, J.O. (2006) Eukaryotic initiation factor 2alpha-independent pathway of stress granule induction by the natural product pateamine A. *J. Biol. Chem.*, **281**, 32870–32878.
- Emara, M.M., Fujimura, K., Sciaranghella, D., Ivanova, V., Ivanov, P. and Anderson, P. (2012) Hydrogen peroxide induces stress granule formation independent of eIF2α phosphorylation. *Biochem. Biophys. Res. Commun.*, **423**, 763–769.

41. Banani, S.F., Rice, A.M., Peeples, W.B., Lin, Y., Jain, S., Parker, R. and Rosen, M.K. (2016) Compositional control of phase-separated cellular bodies. *Cell*, **166**, 651–663.
42. Mateju, D., Eichenberger, B., Voigt, F., Eglinger, J., Roth, G. and Chao, J.A. (2020) Single-molecule imaging reveals translation of mRNAs localized to stress granules. *Cell*, **183**, 1801–1812.
43. Kedersha, N., Stoecklin, G., Ayodele, M., Yacono, P., Lykke-Andersen, J., Fritzler, M.J., Scheuner, D., Kaufman, R.J., Golan, D.E. and Anderson, P. (2005) Stress granules and processing bodies are dynamically linked sites of mRNP remodeling. *J. Cell Biol.*, **169**, 871–884.
44. Ivanov, P., Kedersha, N. and Anderson, P. (2019) Stress granules and processing bodies in translational control. *Cold Spring Harb. Perspect. Biol.*, **11**, a032813.
45. Mollet, S., Cougot, N., Wilczynska, A., Dautry, F., Kress, M., Bertrand, E. and Weil, D. (2008) Translationally repressed mRNA transiently cycles through stress granules during stress. *Mol. Biol. Cell*, **19**, 4469–4479.
46. Ohn, T., Kedersha, N., Hickman, T., Tisdale, S. and Anderson, P. (2008) A functional RNAi screen links O-GlcNAc modification of ribosomal proteins to stress granule and processing body assembly. *Nat. Cell Biol.*, **10**, 1224–1231.
47. Stoecklin, G. and Kedersha, N. (2013) Relationship of GW/P-bodies with stress granules. *Adv. Exp. Med. Biol.*, **768**, 197–211.
48. Wilczynska, A., Aigueperse, C., Kress, M., Dautry, F. and Weil, D. (2005) The translational regulator CPEB1 provides a link between dcp1 bodies and stress granules. *J. Cell Sci.*, **118**, 981–992.
49. Moon, S.L., Morisaki, T., Khong, A., Lyon, K., Parker, R. and Stasevich, T.J. (2019) Multicolour single-molecule tracking of mRNA interactions with RNP granules. *Nat. Cell Biol.*, **21**, 162–168.
50. Buchan, J.R., Muhlrud, D. and Parker, R. (2008) P bodies promote stress granule assembly in *Saccharomyces cerevisiae*. *J. Cell Biol.*, **183**, 441–455.
51. Kroschwald, S., Maharana, S., Mateju, D., Malinowska, L., Nüske, E., Poser, I., Richter, D. and Alberti, S. (2015) Promiscuous interactions and protein disaggregases determine the material state of stress-inducible RNP granules. *Elife*, **4**, e06807.
52. Kershaw, C.J., Nelson, M.G., Lui, J., Bates, C.P., Jennings, M.D., Hubbard, S.J., Ashe, M.P. and Grant, C.M. (2021) Integrated multi-omics reveals common properties underlying stress granule and P-body formation. *RNA Biol.*, **18**, 655–673.
53. Jain, S. and Parker, R. (2013) The discovery and analysis of P Bodies. *Adv. Exp. Med. Biol.*, **768**, 23–43.
54. Protter, D.S.W., Rao, B.S., Van Treeck, B., Lin, Y., Mizoue, L., Rosen, M.K. and Parker, R. (2018) Intrinsically disordered regions can contribute promiscuous interactions to RNP granule assembly. *Cell Rep.*, **22**, 1401–1412.
55. Sanders, D.W., Kedersha, N., Lee, D.S.W., Strom, A.R., Drake, V., Riback, J.A., Bracha, D., Eeftens, J.M., Iwanicki, A., Wang, A. *et al.* (2020) Competing protein-RNA interaction networks control multiphase intracellular organization. *Cell*, **181**, 306–324.
56. Van Treeck, B. and Parker, R. (2018) Emerging roles for intermolecular RNA-RNA interactions in RNP assemblies. *Cell*, **174**, 791–802.
57. Tauber, D., Tauber, G., Khong, A., Van Treeck, B., Pelletier, J. and Parker, R. (2020) Modulation of RNA condensation by the DEAD-Box protein eIF4A. *Cell*, **180**, 411–426.
58. Markmiller, S., Soltanieh, S., Server, K.L., Mak, R., Jin, W., Fang, M.Y., Luo, E.C., Krach, F., Yang, D., Sen, A. *et al.* (2018) Context-dependent and disease-specific diversity in protein interactions within stress granules. *Cell*, **172**, 590–604.
59. Hilliker, A. (2012) Analysis of RNA helicases in P-bodies and stress granules. *Methods Enzymol.*, **511**, 323–346.
60. Cordin, O., Banroques, J., Tanner, N.K. and Linder, P. (2006) The DEAD-box protein family of RNA helicases. *Gene*, **367**, 17–37.
61. Linder, P. and Jankowsky, E. (2011) From unwinding to clamping - the DEAD box RNA helicase family. *Nat. Rev. Mol. Cell Biol.*, **12**, 505–516.
62. Ostareck, D.H., Naarmann-de Vries, I.S. and Ostareck-Lederer, A. (2014) DDX6 and its orthologs as modulators of cellular and viral RNA expression. *Wiley Interdiscip. Rev. RNA*, **5**, 659–678.
63. Weston, A. and Somerville, J. (2006) Xp54 and related (DDX6-like) RNA helicases: roles in messenger RNP assembly, translation regulation and RNA degradation. *Nucleic Acids Res.*, **34**, 3082–3094.
64. Sarkar, M. and Ghosh, M.K. (2016) DEAD box RNA helicases: crucial regulators of gene expression and oncogenesis. *Front. Biosci. (Landmark Ed.)*, **21**, 225–250.
65. Ernault-Lange, M., Baconnais, S., Harper, M., Minshall, N., Souquere, S., Boudier, T., Bénard, M., Andrey, P., Pierron, G., Kress, M. *et al.* (2012) Multiple binding of repressed mRNAs by the P-body protein Rck/p54. *RNA*, **18**, 1702–1715.
66. Serman, A., Le Roy, F., Aigueperse, C., Kress, M., Dautry, F. and Weil, D. (2007) GW body disassembly triggered by siRNAs independently of their silencing activity. *Nucleic Acids Res.*, **35**, 4715–4727.
67. Ozgur, S., Basquin, J., Kamenska, A., Filipowicz, W., Standart, N. and Conti, E. (2015) Structure of a human 4E-T/DDX6/CNOT1 complex reveals the different interplay of DDX6-binding proteins with the CCR4-NOT complex. *Cell Rep.*, **13**, 703–711.
68. Tritschler, F., Braun, J.E., Eulalio, A., Truffault, V., Izaurralde, E. and Weichenrieder, O. (2009) Structural basis for the mutually exclusive anchoring of P body components EDC3 and Tral to the DEAD box protein DDX6/Me31B. *Mol. Cell*, **33**, 661–668.
69. Pitchaiya, S., Mourao, M.D.A., Jalihal, A.P., Xiao, L., Jiang, X., Chinnaiyan, A.M., Schnell, S. and Walter, N.G. (2019) Dynamic recruitment of single RNAs to processing bodies depends on RNA functionality. *Mol. Cell*, **74**, 521–533.
70. Collart, M.A. (2016) The Ccr4-Not complex is a key regulator of eukaryotic gene expression. *Wiley Interdiscip. Rev. RNA*, **7**, 438–454.
71. Di Stefano, B., Luo, E.C., Haggerty, C., Aigner, S., Charlton, J., Brumbaugh, J., Ji, F., Rabano Jiménez, I., Clowers, K.J., Huebner, A.J. *et al.* (2019) The RNA helicase DDX6 controls cellular plasticity by modulating P-body homeostasis. *Cell Stem Cell*, **25**, 622–638.
72. Song, H. and Ji, X. (2019) The mechanism of RNA duplex recognition and unwinding by DEAD-box helicase DDX3X. *Nat. Commun.*, **10**, 3085.
73. Absmeier, E., Santos, K.F. and Wahl, M.C. (2020) Molecular mechanism underlying inhibition of intrinsic ATPase activity in a Ski2-like RNA helicase. *Structure*, **28**, 236–243.
74. Wang, X., Chang, L., Wang, H., Su, A. and Wu, Z. (2017) Dcp1a and GW182 induce distinct cellular aggregates and have different effects on microRNA pathway. *DNA Cell Biol.*, **36**, 565–570.
75. Liu, Z., Johnson, S.T., Zhang, Z. and Corey, D.R. (2019) Expression of TNRC6 (GW182) proteins is not necessary for gene silencing by fully complementary RNA duplexes. *Nucleic Acid Ther.*, **29**, 323–334.
76. Bourgeois, C.F., Mortreux, F. and Auboeuf, D. (2016) The multiple functions of RNA helicases as drivers and regulators of gene expression. *Nat. Rev. Mol. Cell Biol.*, **17**, 426–438.
77. Mugler, C.F., Hondele, M., Heinrich, S., Sachdev, R., Vallotton, P., Koek, A.Y., Chan, L.Y. and Weis, K. (2016) ATPase activity of the DEAD-box protein Dhh1 controls processing body formation. *Elife*, **5**, e18746.
78. Kamenska, A., Simpson, C., Vindry, C., Broomhead, H., Bénard, M., Ernault-Lange, M., Lee, B.P., Harries, L.W., Weil, D. and Standart, N. (2016) The DDX6-4E-T interaction mediates translational repression and P-body assembly. *Nucleic Acids Res.*, **44**, 6318–6334.
79. Ito, K., Takahashi, A., Morita, M., Suzuki, T. and Yamamoto, T. (2011) The role of the CNOT1 subunit of the CCR4-NOT complex in mRNA deadenylation and cell viability. *Protein Cell*, **2**, 755–763.
80. Marnef, A., Weil, D. and Standart, N. (2012) RNA-related nuclear functions of human Pat1b, the P-body mRNA decay factor. *Mol. Biol. Cell*, **23**, 213–224.
81. Mathys, H., Basquin, J., Ozgur, S., Czarnocki-Cieciura, M., Bonneau, F., Aartse, A., Dziembowski, A., Nowotny, M., Conti, E. and Filipowicz, W. (2014) Structural and biochemical insights to the role of the CCR4-NOT complex and DDX6 ATPase in microRNA repression. *Mol. Cell*, **54**, 751–765.
82. Li, Y., Chen, R., Zhou, Q., Xu, Z., Li, C., Wang, S., Mao, A., Zhang, X., He, W. and Shu, H.B. (2012) LSM14A is a processing body-associated sensor of viral nucleic acids that initiates cellular antiviral response in the early phase of viral infection. *Proc. Natl. Acad. Sci. U.S.A.*, **109**, 11770–11775.
83. Brandmann, T., Fakim, H., Padamsi, Z., Youn, J.Y., Gingras, A.C., Fabian, M.R. and Jinek, M. (2018) Molecular architecture of LSM14 interactions involved in the assembly of mRNA silencing complexes. *EMBO J.*, **37**, e97869.

84. Jain,S., Wheeler,J.R., Walters,R.W., Agrawal,A., Barsic,A. and Parker,R. (2016) ATPase-modulated stress granules contain a diverse proteome and substructure. *Cell*, **164**, 487–498.
85. Cirillo,L., Cieren,A., Barbieri,S., Khong,A., Schwager,F., Parker,R. and Gotta,M. (2020) UBAP2L forms distinct cores that act in nucleating stress granules upstream of G3BP1. *Curr. Biol.*, **30**, 698–707.
86. Liu,J., Liu,Z. and Corey,D.R. (2018) The requirement for GW182 scaffolding protein depends on whether argonaute is mediating translation, transcription, or splicing. *Biochemistry*, **57**, 5247–5256.
87. Sachdev,R., Hondele,M., Linsenmeier,M., Vallotton,P., Mugler,C.F., Arosio,P. and Weis,K. (2019) Pat1 promotes processing body assembly by enhancing the phase separation of the DEAD-box ATPase Dhh1 and RNA. *Elife*, **8**, e41415.
88. Balak,C., Benard,M., Schaefer,E., Iqbal,S., Ramsey,K., Ernoult-Lange,M., Mattioli,F., Llaci,L., Geoffroy,V., Courel,M. *et al.* (2019) Rare de novo missense variants in RNA helicase DDX6 cause intellectual disability and dysmorphic features and lead to P-body defects and RNA dysregulation. *Am. J. Hum. Genet.*, **105**, 509–525.